ARTICLE

Geology, geochemistry and petrology of basalts from Paraná Continental Magmatic Province in the Araguari, Uberlândia, Uberaba and Sacramento regions, Minas Gerais state, Brazil

Geologia, geoquímica e petrologia de basaltos da Província Magmática Continental do Paraná nas regiões de Uberlândia, Araguari, Uberaba e Sacramento, Minas Gerais

Lucia Castanheira de Moraes[1], Hildor José Seer[1]*, Leila Soares Marques[2]

ABSTRACT: *This study covers the region between the cities of Sacramento and Araguari/Uberlândia (Minas Gerais State, Brazil), where basalt flows from the Paraná Continental Magmatic Province outcrop. The investigated rocks present tholeiitic signature, with high titanium content, and are classified as Pitanga magma-type. The preserved basalt thickness is between 10 and 200 meters and individual flows do not exceed 15 meters thick. Flows were identified as sheet lobes, smaller and thinner flows units — stacked laterally and vertically forming compound lavas —, or frontal, centimetric lobes. The basalt flows show decimetric to metric intercalations of clastic sedimentary rock, with depositional characteristics that can vary from aeolian to lacustrine, and are important markers on prevailing environmental conditions. The plagioclases are dominantly labradorite and pyroxene is augite, whereas olivine can be hyalosiderite or hortonolite/ferrohortonolite. The behavior of the major, minor and trace elements is compatible with the presence of at least two parental magmas, which were subjected to fractional crystallization mainly of plagioclase, clinopyroxene, ilmenite and magnetite. There is a chemistry distinction between basalts from Sacramento to those from Araguari/Uberlândia region, the former one showing more evolved than the last one. The high (La/Lu)N values are indicative of partial melting of a garnet peridotite, while the Rare Earth Elements (REE) values are indicative of fractional crystallization.*

KEYWORDS: *Paraná-Etendeka Province; Lithostratigraphy; Petrography; Lithochemistry; Mineral chemistry.*

INTRODUCTION

Continental flood basalt provinces are huge eruptive events characterized by their phenomenal volumes of tholeiitic basalts erupted in a very short time range and in a continental environment from fissure systems in the Earth's crust (Hooper 2000). One of these, the Paraná-Etendeka Province (PEP), associated with the opening of the South Atlantic Ocean (Renne *et al.* 1992, Peate *et al.* 1992, Turner *et al.* 1994), occupies an estimated area of 1,300,000 km² distributed across Brazil, Argentina, Uruguay, Paraguay and Namibia (Fig. 1).

The Brazilian portion of the PEP volcanic rocks (Serra Geral Group; Rossetti *et al.* 2017) was formed in the final phase of the Paraná Basin. This was an intracratonic and polyhistoric basin, which was part of the Gondwana Continent, dominated in its interior, at that time, by the arid climate (Scherer 2002, Jerram & Stollhofen 2002). These volcanic rocks are mainly of basaltic composition and overlap the aeolian deposits of the Botucatu Formation, and, in some places, they are intercalated. Sills, mainly located in the northern area, as well as the mafic dyke swarms of Ponta Grossa, Serra do Mar and Florianópolis, are associated to

the volcanism (Ernesto *et al.* 2002), and together the extrusive and intrusive rocks compose the Paraná Continental Magmatic Province (PCMP). The intrusive rocks are predominantly basic in composition (micro-gabros), and all of them show similar geochemical characteristics to the associated volcanic rocks (Bellieni *et al.* 1984, Piccirillo *et al.* 1990, Ernesto *et al.* 1999).

The PCMP is dominated by tholeiitic basalts and andesibasalts (> 90%), although significant quantities of two compositionally distinct groups of silicic volcanics — Palmas (dacites and rhyolites with low-Ti content) and Chapecó types (dacites with higher-Ti content) — are found along the southern and eastern parts of the province (Mantovani *et al.* 1985, Bellieni *et al.* 1986, Piccirillo & Melfi 1988, Peate 1997). Peate *et al.* (1992) subdivided mafic magmatism into six types (Fig. 1A): Urubici, Pitanga, Paranapanema (high TiO$_2$) and Gramado, Esmeralda and Ribeira (low TiO$_2$). The northern PCMP is dominated by Pitanga and Paranapanema basalts, whereas the Gramado and Esmeralda tholeiites occur in southern PCMP. The Ribeira and Urubici flows are scarce

and occur in the northern and southern PCMP, respectively. Recent studies have shown that some Urubici flows are present in the border region between Minas Gerais and São Paulo states (Machado 2005), as well as dikes crosscutting rocks of the São Francisco Craton, Minas Gerais (Seer *et al.* 2011, Marques *et al.* 2016). The age of the main phase of the volcanic activity is concentrated at 134 to 132 Ma, according with data obtained by Renne *et al.* (1992), Thiede and Vasconcelos (2010), and Janasi *et al.* (2011).

The regional location of the study area is shown in Figure 1B. It is also possible to see the current limits of the PCMP and the stratigraphic column for the Triângulo Mineiro region, Minas Gerais state, in the northeast of the province. Most of the basalts of the PCMP is covered by fluvio-lacustrine sedimentary Upper Cretaceous rocks belonging to the Bauru Basin. The analyzed samples, as well as some by Rocha-Júnior *et al.* (2013) used for comparison (KS samples), are located in Figure 1C. Much of the information available today from the northern portion of the PCMP is restricted to lithochemical data, without any knowledge of
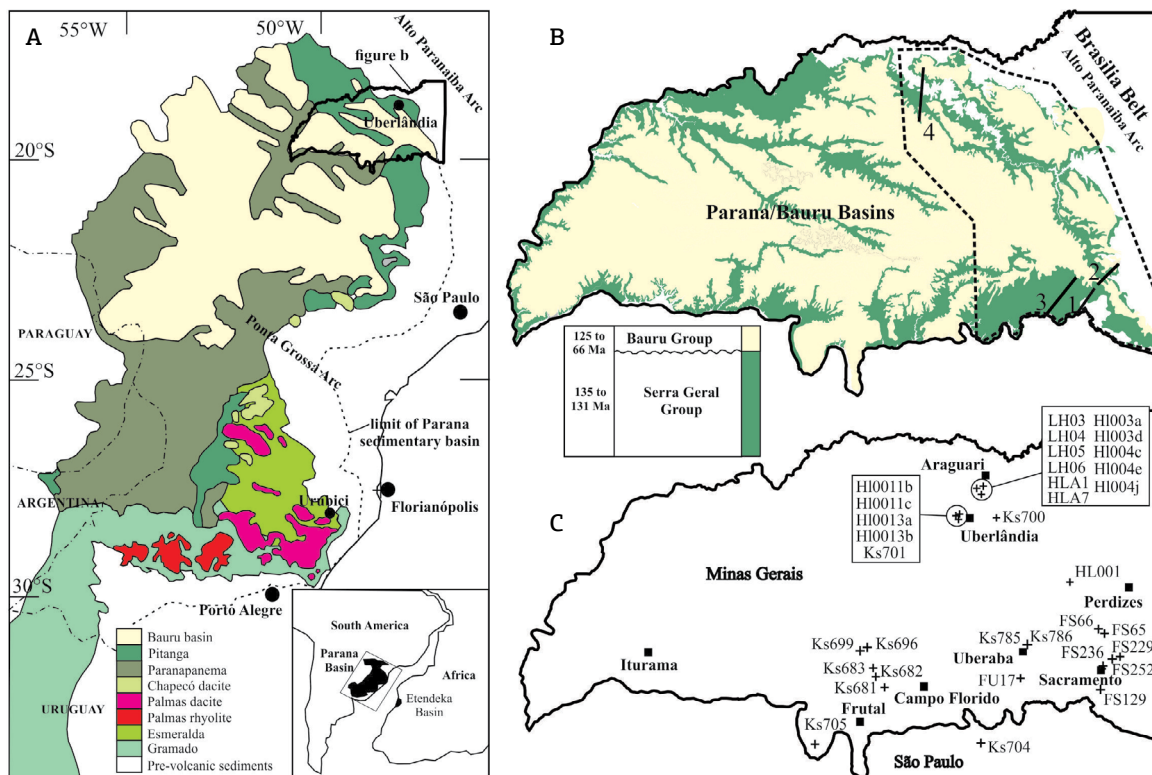

Figure 1. (A) Geological illustration of the Paraná Continental Magmatic Province (PCMP) with its magmatic rocks distribution overlapped by the Bauru Basin. Urubici and Ribeira type magma occurrences are not compatible with this scale. In detail, sketch of the Paraná-Etendeka Province (PEP). Modified from Janasi *et al.* (2011) and Waichel (2006); (B) geologic map of the Triângulo Mineiro region, modified from Pinto and Silva (2014); 1, 2, 3 and 4 are geologic sections represented in Figure 2. Dashed line limits the studied area; (C) location of analyzed samples and cities of the Triângulo Mineiro region mentioned in the text.

the lithostratigraphic point of view, with the exception of the works by Araujo (1982), Ferreira (1985), Machado (2005), Pacheco *et al.* (2017) and Moraes and Seer (2017). The Triângulo Mineiro region is limited by the Alto Paranaíba Arch, a regional topographic high present at least from the Lower Cretaceous and tectonically reactivated during the Upper Cretaceous and Cenozoic. The Alto Paranaíba Arch (Fig. 1A) composes the northeast border of the PCMP and hosts a series of dykes with NW direction and alkaline-carbonatite bodies of Upper Cretaceous age. The NW lineaments, inherited from the Neoproterozoic structure of the region, control the directions of the dykes. According to preliminary petrographic and geochemical data, dykes are potential feeders of the PCMP volcanism in the area. The Alto Paranaíba Arch was the source area of sediments of both, the Botucatu Formation and the Bauru Basin (Hasui 1967, Barcelos 1989, Batezelli 2003), besides an important watershed in the Triângulo Mineiro. It also seems to have behaved as a geographic barrier controlling the climate and the advance of the dunes and lavas of the PCMP.

GEOLOGICAL CONTEXT

The map of isopacs for the PCMP volcanic rocks in the Triângulo Mineiro region (Batezelli 2003, p. 147) shows a thickness over 1,000 meters in the west (Iturama in Fig. 1C) that decreases eastwards, being less than 100 meters in the Sacramento region. This information can be confirmed in

Figure 2, in which both the paleotopography and the lithology distribution of the Botucatu Formation and PCMP volcanic rocks are represented.

Figure 2 shows an irregular paleotopography, higher in the direction of the Alto Paranaíba Arch, to the northeast. The thickness of sandstones and basalts and the relationships between them are variable. The occupation of the paleorelief begins with the sedimentation in paleovalleys by aeolian sandstones of the Botucatu Formation, whose thicknesses vary from less than two to 110 meters. In the Sacramento region, sections 1 and 2 show dunes over the basement and several aeolian sandstone lenses interspersed in basalt (Figs. 3A and 3B). Between Sacramento and Uberaba, section 3 shows no basal dunes, but many aeolian sandstone lenses. In the Uberlândia/Araguari region (section 4), just two small dunes occur to the north of Araguari city. On the other hand, lenses of alluvial fan and lacustrine deposits are present (Figs. 3C and 3D).

Alluvial fans occur as conglomerate levels dominantly matrix supported and can reach thicknesses of about 1 meter in recurrent channeled shapes. Lacustrine deposits are limited in area and thickness — with minimum length and depth of 50 and 2 meters, respectively —, and cover alluvial fans or interspersed basalt flows. Ostracod fossils were found in three of the four lacustrine deposits. Fossilized conifer woods were described in Botucatu Formation, near Uberlândia city (Pires *et al.* 2011).

The lavas also fill topographical depressions and free spaces between dunes, and the preserved thickness is between 10 and
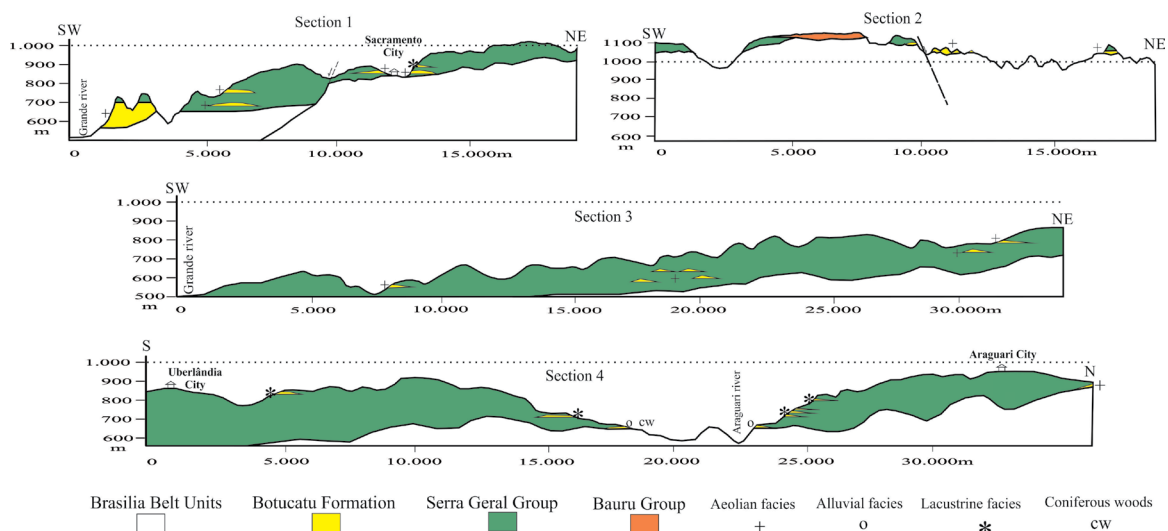
Source: modified from Moraes and Seer, 2017.

Figure 2. Paleorelief of the NE limit of the Paraná Continental Magmatic Province (PCMP) represented in regional geologic cross-sections (location on Figure 1B). The relation between basalts from PCMP and aeolian (+), alluvial (o) and lacustrine (*) dominant sediments of the Botucatu Formation are made explicit.

200 meters. The contact between sedimentary and basaltic rocks is concordant. Locally it is possible to see interaction between lavas and sand forming peperites/pseudopeperites, degassing pipes in sandstone and grooves produced by basalt flows on still unconsolidated surface (Figs. 4A, 4B, 4C and 4D). The intertrapp sandstone can vary from a few centimeters to a few meters — and may occupy the voids between the upper crust blocks of a pahoehoe flow —, indicating the intermittent nature of the two processes. Nevertheless, these recurring intercalations indicate that aeolian processes and volcanism occurred simultaneously.

Taking into account the quality and extent of the outcrops and the scale studied, it was not possible to determine the actual size of the lava flows. The outcrops visited do not exceed 15 meters thick. Lobes are found in sheet, structured in lava core and fractured crust facies (Fig. 5A), as well as smaller and thinner flows units, < 2 meters thick, stacked laterally and vertically forming compound lavas (Fig. 5B). Small frontal lobes, centimetric, similar to toes, were also identified in loose blocks or as grooves on the upper crust pahoehoe and on still unconsolidated sandstone surface (Figs. 5C and 5D).

Sheet flows are exposed in basalt quarries. Colonnade usually occurs in the first third from the base of the flow, < 2 m thick, and eventually is also exposed near the top. Entablature of aphanitic basalt dominates lava flows, being narrower (< 30 cm wide), irregular and twisted. Fan radiate

columns can be present (Fig. 5E) and exhibit a nucleus infilled with brecciated and hydrothermally altered material. The brecciated rubble top of the flow has abrupt contacts with the underlying entablature unit via decimetric chill-zone. In general, this level is rich in vesicles/amygdales that can be flattened or spherical. They vary between 0.5 and 1 cm in diameter and are filled by silica, calcite, zeolites, or celadonite, which is predominant. At the entablature rubbly-top transition, gas blisters (5 to 25 cm) that can be flattened, infilled with chalcedony and quartz, ± calcite crystals occur. The rubbly surface of the flow hardly exceeds 1 meter in length and consists of clasts of basalt within a fragmental basalt matrix-supported breccia. Alternatively, the clasts may be highly vesicular scoria and the spaces between the fragments may be filled by aeolian sand or cemented by carbonate.

Noteworthy is the presence of two sets of pillow lavas (5.7 and 7.4 meters average thickness, respectively) that interact with fluvio-lacustrine sediments in area situated between the cities of Uberlândia and Araguari, along the Central Atlantic Railway (FCA), in a location known as Fundão (Moraes & Seer 2017). This interaction gives rise to peperites as interpillow material, which may also be formed by hyaloclastite and fragments of lava, intrinsically mixed to the sediments in a complex way. The basal set of pillows, sized between 30 to over 150 centimeters, with hollow or filled center, is well
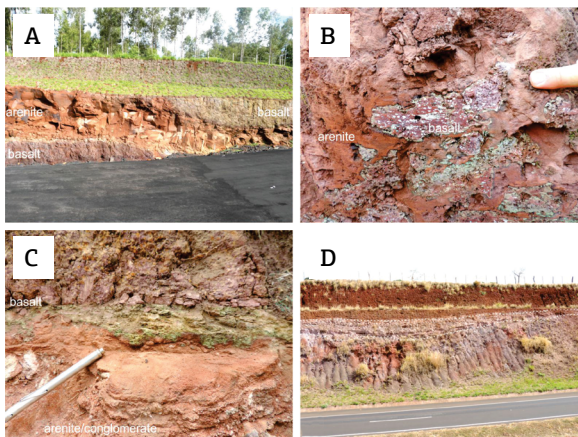

Figure 3. Sedimentary rocks of the Botucatu Formation and their field relations. (A) Aeolian sandstone lenses interspersed with basalt flows; (B) aeolian sandstone occupying voids in the upper crust blocks of basalt flow; (C) alluvial fan matrix supported conglomerate and sandstone from the Botucatu Formation overlaid by lava flow in irregular contact. The light green layer at the base of the lava flow represents rapid quenching of the lava, already altered; (D) lacustrine deposit (white dashed line) interspersed with lava flow.
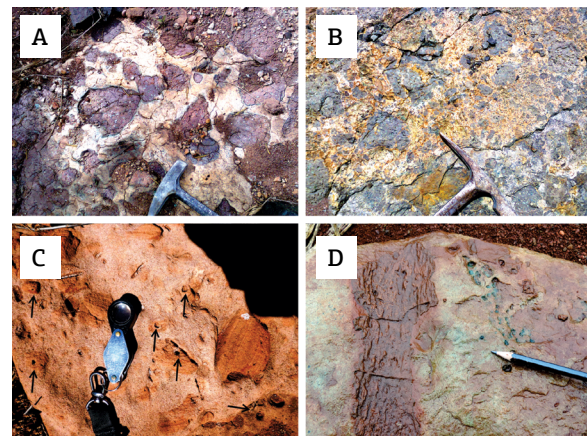
Figure 4. Sediment/lava field relationships: (A) heavily weathered peperite, with rounded fragments of oxidized-aphanitic basalt that has clay-sandy infilled vesicles in the mid of a clay-sandy matrix. Fragment edges show a reaction rim; (B) brecciated rubble surface filled by aeolian sand or cemented by carbonate/zeolite/chalcedony. The field relationship allow distinguishing both A and B structures; (C) blister of degassing in fractured sandstone due to lava flow action; (D) grooves and basalt remnants due to the passage of small lava lobes in still unconsolidated sandstone surface.

preserved, and the pillows have chilled rim. The upper set is heavily weathered, and pillows are wrapped in fragments of sandstone, sandy mudrock and mudrock, but show compact arrangement — unlike the basal set, that may show high or very low packaging.

In general, the basalt is fine-grained to aphanitic, with a dark-gray to a greenish-dark gray color, sometimes reddish due to weathering, and consists of microphenocrysts of plagioclase and pyroxene and, less commonly, olivine. The mesostasis is dominated by crystals of plagioclase, pyroxene, magnetite, maghemite and ilmenite. There is a difference between textures of entablature and colonnade basalts; in the former one, volcanic glass is conspicuous, microlites are abundant, opaque crystals are predominantly skeletal, and swallowtail-like textures are common in plagioclase (Fig. 6A). On the other hand, colonnade basalts have phenocrysts with euhedral tendency, sometimes zoned, and coarser mesostasis in predominantly intergranular texture, sub- to euhedral opaque minerals and interstitial and localized glass (Fig. 6B). Where present, microvesicules/microamygdales (< 2 mm) are spherical to irregular, dominantly filled by celadonite, but also by silica, zeolites and calcite (Fig. 6C). The borders of basalt flows tend to be vitreous, with dispersed euhedral crystals of plagioclase and clinopyroxene and amoeboid vesicles (Fig. 6D).

MATERIALS AND METHODS

The petrographic studies were performed on 28 polished thin sections at the Centro de Pesquisas Professor Manoel Teixeira da Costa of the Geoscience Institute of the Universidade Federal de Minas Gerais (UFMG). The minerals were analyzed by electronic microprobe in the laboratories of the Universidade Federal de Goiás (UFG) (153 analyses) and the Universidade Estadual Paulista "Júlio de Mesquita Filho" (UNESP) (252 analyses), of which 113 in pyroxene, 184 in plagioclase, 88 in oxides, 9 in olivine and 11 in alteration minerals. The polished thin sections were carbon film coated, and analytical work was performed at 15 kV and 20 nA. The data were processed using the Gabbrosoft Project worksheets (http://www.gabbrosoft.org), the WinPyrox (Yavuz 2013) and the Igpet software.

Whole-rock chemical analysis of four samples for major, minor, trace and rare earth elements were performed at Geosol laboratories, while 17 at UNESP ones. The percent differences for major and minor elements of sample HL004C (analyzed at GEOSOL and at UNESP) are lower than 4.8%, indicating that the results are compatible, without analytical bias. Samples were crushed, split and pulverized in mechanical agate mortar. At UNESP, they were analyzed by *X-ray fluorescence* (*XRF*) after $Li_2B_4O_7/LiBO_2$
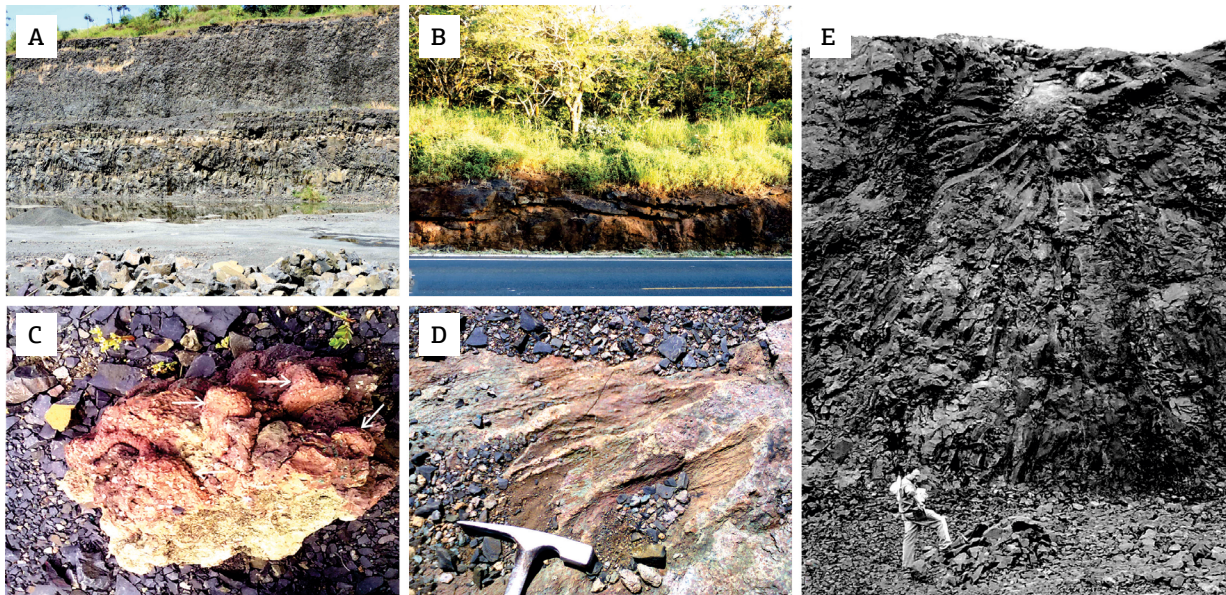
Figure 5. Characteristics of basaltic flows: (A) sheet flows with many lobes. Note short but well developed colonnade at the base flows and entablature, which is dominant and extremely fractured; (B) compound lavas formed by thinner, smaller lava units stacked up; (C) small basalt toes, rusty and vesicular, flowing through the void spaces of a brecciated rubbly surface. Well-formed crystals of analcime can be seen in both; (D) grooves of small lava lobes on the top of brecciated pahoehoe flow. Note the breccia crust was still unconsolidated when the basaltic lobes flowed over it; (E) fan radiated columns from a core infilled with brecciated and hydrothermalized material.

fusion and LOI determined by gravimetric analysis (Nardy *et al.* 1997). At GEOSOL, major elements were analyzed by inductively coupled plasma optical emission spectrometry (ICP-OES); minor and trace elements by inductively coupled plasma mass spectrometry (ICP-MS). The relative accuracy for major and minor elements in both laboratories is 1%, whereas for trace elements it is within ± 3%. Major oxide contents were recalculated to 100% on an anhydrous basis. The data were processed and plotted using the softwares Igpet and Petrograph (Petrelli *et al.* 2005).

MINERAL CHEMISTRY

Modal mineralogy is on average 51% plagioclase, 36% pyroxene, 7% oxides and 4% olivine, which, however, may reach 6% or be absent. This result is consistent with the norms calculated for the chemically analyzed samples, where five samples have normative olivine and 17 do not. In the latter one, normative quartz is present. Normative apatite and ilmenite occurs in all samples.

The Ab-Or-An diagram (Fig. 7) shows the result of the analysis of 100 microphenocrysts and 41 microlites of plagioclase (Tab. 1). Some plagioclases are characterized by compositional zoning (Figs. 8A and 8B) and, when it occurs, their core and edge were analyzed separately. Among the micro-phenocrysts analyzed, sample HL002 has the most calcic crystal ($An_{75}Ab_{24}Or_1$), while the HL003b ($An_{51}Ab_{46}Or_3$), the least one. In mesostasis, the variations are between $An_{63}Ab_{35}Or_2$ (HL002) and $An_{47}Ab_{49}Or_4$ (HL003b), in a coherent and expected way. Although normal zonation is present (for example in HL004c sample), reverse zoning occurs too, and in some of the analyzed samples the nuclei of micro-phenocrysts are less calcic than those ones of the mesostasis. Fig. 9 shows edge-to-edge profiles for two zoned micro-phenocrysts. Profile A (FU463) shows composition An_{68} at the edges and An_{47} at the core. Profile B (FU687b) shows rims with composition around An_{48}, depletion in calcium to $An_{46.5}$ followed by enrichment, reaching the core with An_{50}. Although the variation is small, it draws attention to a complex magmatic trajectory.

The composition of 37 micro-phenocrysts and 30 microlites of pyroxenes is shown in Fig. 10A, the Wo-En-Fs ternary diagram (Morimoto 1988), and Table 2 shows some representative analyses and formulae of them. With the exception of two crystals from LH04 sample that fall in the pigeonite field, all the other pyroxenes analyzed are augites. Fig. 10B shows the compositional variation profiles obtained in zoned micro-phenocrysts. A normal variation, with enrichment in Fs towards the rim, is prevailing, except for the micro-phenocrysts present in samples HL004B1, HL004B2, LH04-2 and LH04-3. In these ones, some micro-phenocrysts are

Pl: plagioclase; cpx: clinopyroxene; op: opaque mineral; g: glass; v: vesicle.

Figure 6. Representative features in thin sections. (A) Plagioclase and olivine (altered to iddingsite) phyric basalt with acicular plagioclase crystals and seeds of clinopyroxene in the middle of indistinguishable oxides and glassy matrix. Parallel polarizers; (B) magnetite and augite intergranular to plagioclase crystals and sub-ophitic texture in fine-grained basalt with subordinated glass. Parallel polarizers; (C) fine-grained basalt with spherical vesicle filled with celadonite and silica. Crossed polarizers; (D) amoeboid amygdule, filled with celadonite and silica, set in a vitreous mesostasis and sparse pyroxene and plagioclase crystals, ≤ 0.5 mm, which may be zoned. Parallel polarizers.
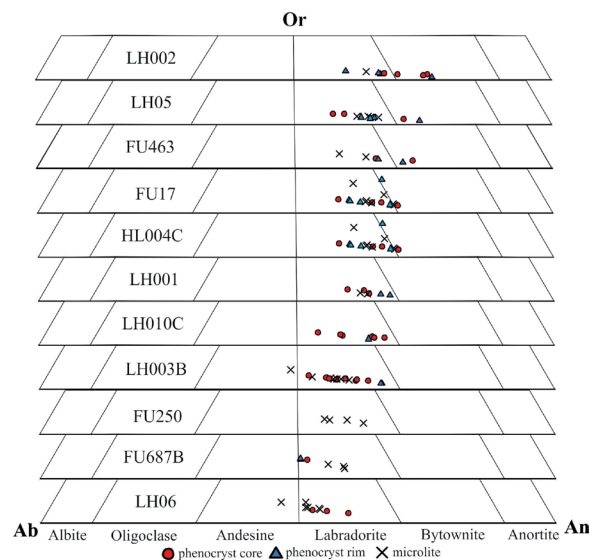

Figure 7. Compositional variation of plagioclase of the basalt flows (Pitanga magma type) studied according Or-Ab-An diagram of Deer *et al.* (2003).

Table 1. Representative analysis and formulae of plagioclase.

| Sample	FU17 P C	FU17 P R	FU17 MP C	HL001 P C	HL001 P R	HL001 MP C	HL004c P C	HL004c P R	HL004c MP C	LH05 P C	LH05 P R	LH05 M PC
Component												
SiO_2	50.580	53.330	52.330	52.400	51.150	52.320	50.420	52.970	54.220	53.430	51.860	51.530
TiO_2	0.110	0.170	0.130	0.000	0.000	0.000	0.000	0.000	0.000	0.000	0.000	0.000
Al_2O_3	30.080	27.840	28.880	30.220	30.650	29.950	31.320	29.310	28.430	29.140	30.340	30.440
FeO_t	0.850	0.920	0.930	0.730	0.870	0.790	0.800	0.750	0.970	0.750	0.730	0.860
CaO	13.380	11.390	11.920	12.830	13.600	12.730	14.370	12.060	11.240	11.860	13.140	12.910
Na_2O	3.140	4.070	3.690	3.910	3.480	3.950	3.090	4.200	4.790	4.360	3.760	3.840
K_2O	0.280	0.500	0.430	0.290	0.240	0.280	0.240	0.380	0.460	0.370	0.280	0.290
Total	98.420	98.220	98.310	100.380	99.990	100.020	100.240	99.670	100.110	99.910	100.110	99.870
Cations based on 32 oxygen												
Si	9.369	9.843	9.663	9.470	9.337	9.519	9.198	9.653	9.831	9.705	9.436	9.405
Ti	0.015	0.024	0.018	0.000	0.000	0.000	0.000	0.000	0.000	0.000	0.000	0.000
Al	6.565	6.057	6.285	6.482	6.593	6.420	6.733	6.294	6.075	6.238	6.506	6.548
Fe(ii)	0.132	0.143	0.143	0.111	0.133	0.121	0.122	0.114	0.147	0.114	0.111	0.131
Ca	2.655	2.252	2.358	2.501	2.660	2.481	2.808	2.354	2.183	2.308	2.561	2.524
Na	1.127	1.456	1.321	1.380	1.232	1.395	1.093	1.483	1.683	1.536	1.326	1.360
K	0.066	0.118	0.101	0.066	0.056	0.066	0.057	0.085	0.107	0.087	0.066	0.067
Cat sum	19.929	19.892	19.888	20.011	20.011	20.001	20.011	19.984	20.026	19.990	20.007	20.034
End-member (%)												
An	69.000	58.870	62.390	63.370	67.370	62.950	70.950	60.010	54.950	58.710	64.780	63.880
Ab	29.290	38.050	34.940	34.950	31.210	35.380	27.620	37.820	42.370	39.090	33.550	34.430
Or	1.710	3.080	2.680	1.680	1.420	1.670	1.430	2.170	2.680	2.200	1.670	1.690

P: phenocryst; MP: micro-phenocryst; C: core; R: rim.

fairly homogeneous or show significant inverted zoning. In general, there is a negligible variation of the chemical composition from the core ($Wo_{35-41}En_{39-47}Fs_{15-24}$) to the rim ($Wo_{36-39}En_{38-47}Fe_{14-23}$) of the zoned micro-phenocrysts, and a trend of differentiation is not identified.

Some subhedral micro-phenocrysts of clinopyroxenes in subophitic texture are shown in Fig. 8C, while in the back-scattered image of Fig. 8D a zoned augite micro-phenocryst with about 0.4 mm in length with subtle zoning can be seen. It partially involves plagioclase crystals, in subophitic texture, and is immersed in mesostasis rich in plagioclase, pyroxene, ilmenite and magnetite microlites, besides glass in the process of devitrification.

Oxides occur as subhedral to euhedral crystals, tabular or skeletal (Figs. 11A and 11B). The ternary FeO *vs.* TiO_2 *vs.* Fe_2O_3 diagram (Akimoto & Katsura 1959) shows the major solid solution series magnetite-ulvöspinel, hematite-ilmenite and ferropseudobrookite-pseudobrookite. The data of the analyzed oxides (Tab. 3 and Fig. 12) plot on the field of ilmenite. The subordinate presence of titanomaghemite (Katsura & Kushiro 1961) suggests weathering or low-T oxidation of titanomagnetite or magnetite. The presence of magnetite was attested by magnet in hand samples.

When present, olivine shows alteration to iddingsite, so that preserved crystals are very rare (Figs. 11C and 11D). Nine olivine crystals of three basaltic samples were analyzed
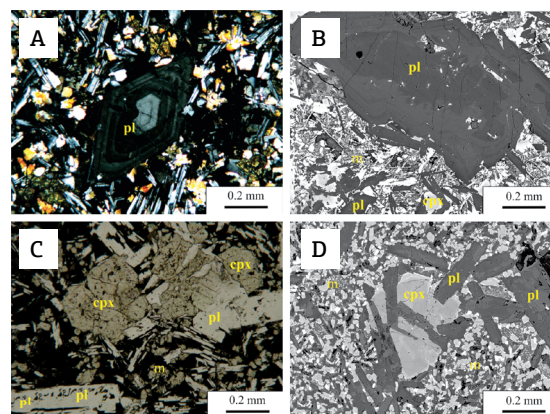
Pl: plagioclase; cpx: clinopyroxene; m: mesostasis.

Figure 8. Microscopic aspects representative of basalt flows. (A) Micro-phenocryst of concentrically zoned labradorite in a mesostasis rich in plagioclase laths and granules of clinopyroxene, magnetite and olivine already transformed into iddingsite. Part of the black material is volcanic glass. Crossed polarizers; (B) back-scattered image showing phenocryst of plagioclase with irregular zoning and inclusions of glass and oxides in sample HL001; (C) augites in micro-phenocrysts, showing inclusions of plagioclase, oxides and glass, and immersed in a mesostasis of clinopyroxene, plagioclase, oxides and glass. Parallel polarizers; (D) back-scattered image of augite in micro-phenocryst with distinct marginal zoning and delicate "patchy zoning" within the crystal.

(Tab. 4, Fig. 13). None of them has significant zonation. FU017 sample shows olivine with a more magnesian composition ($Fo_{59}Fa_{41}$-hyalosiderite), while in samples FU250 and LH05 olivine is markedly ferriferous (between $Fo_{35}Fa_{65}$ and $Fo_{28}Fa_{70}$ — hortonolite/ferrohortonolite) according to Deer *et al.* (2003). Despite this difference in composition, no significant textural distinctions were observed. However, the olivines of sample FU017 are subhedral and slightly rounded, suggesting corrosion, while other ones have more inclusions and almost absence of faces. As for the size, all are about 75 μm in the longest length. The few data available do not allow further consideration.

The presence of glass in the basalts mesostasis is very common, as interstitial and localized form or as significant proportions. In either case, devitrification processes are common, and the presence of crystallites is conspicuous (Figs. 14A and 14B).

ROCK CHEMISTRY

The 22 analyzed samples were divided according to their areal distribution (Tab. 5), being six of them from the Sacramento region, to the southeast, one from the Uberaba area, one from the Perdizes region and 14 from the area between Uberlândia and Araguari cities, to the northwest (see Fig. 1 for location). Table 5 also shows the CIPW Norm for these rocks.

The flows are classified as basalts, in the total alkali-versus-silica (TAS) diagram (Le Bas *et al.* 1986). The SiO_2 concentrations range from 48.10 to 51.81 wt% and total alkalis between 3.43 and 4.49 wt% (Fig. 15), and all samples plot in the field of subalkaline volcanic series (Irvine & Baragar 1971). The rocks have a tholeiitic character, with strong enrichment of iron in relation to alkalis and magnesium (Fe_2O_3t/MgO between 2.6 and 4.0) and high-TiO_2 contents, belonging to the HTi Basalt Group of the PCMP (Bellieni *et al.* 1984, Peate *et al.* 1992).

The main characteristic shown by the variation diagrams of major, minor and trace elements against MgO (Figs. 16 and 17), considered as a magmatic differentiation index, is the separation of two specific fields: one for the more evolved rocks from the Sacramento region, in the southeast of the surveyed area; and the other one for those less evolved rocks from the Uberlândia/Araguari region, at the northwest. The only representative sample of the Uberaba region falls in the intermediate area, between the two groups. Samples from the pillow lavas related basaltic flows behave independently by plotting in between the groups mentioned; four of them overlap the basalts of the Uberlândia/Araguari region, while the other one has lower MgO, SiO_2, Al_2O_3, CaO and Na_2O and overlaps the Sacramento Group. Analyzed together, a negative correlation trend is observed for SiO_2, Na_2O, K_2O, P_2O_5 and (subtle) for TiO_2 and positive for CaO and Al_2O_3. There is a strong correspondence with Rocha-Júnior *et al.* (2013) data, even though those present lower values for Na_2O and higher for Al_2O_3.

According to the parameters proposed by Peate *et al.* (1992), the studied basalts belong to the Pitanga magma
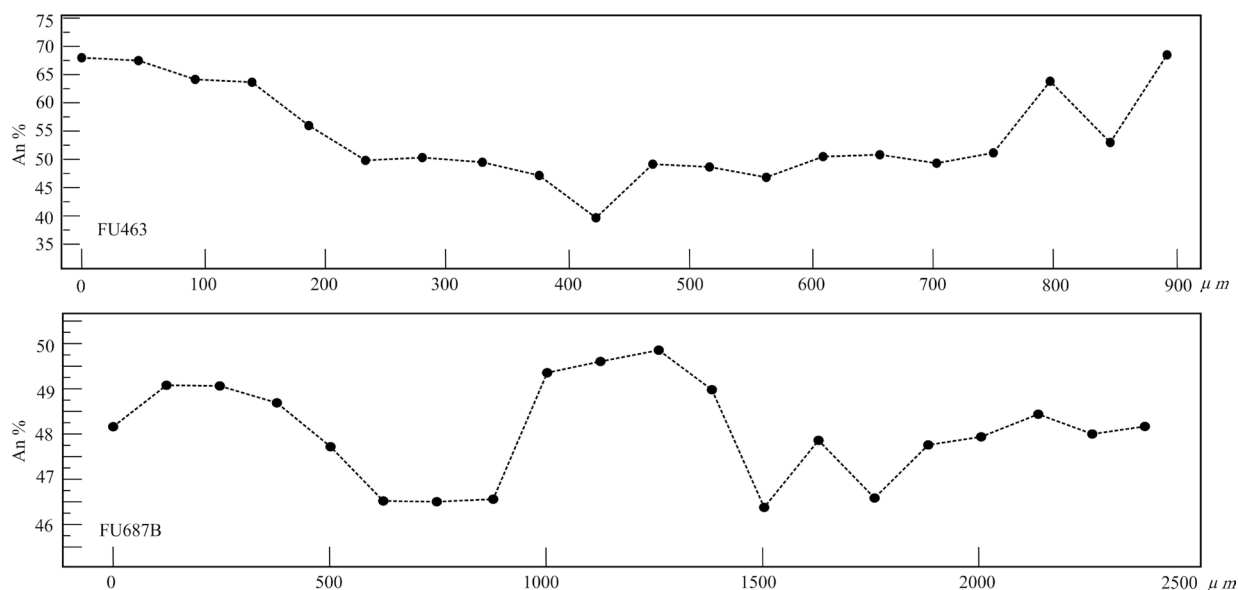

Figure 9. Rim to rim profile in two plagioclase phenocrysts that show very distinct crystallization history. Sample FU 463 shows gradual Ca-enrichment from the center to the edge of the crystal, while the FU687b sample has a more complex history, with a Ca-enriched center and border and a depleted intermediate portion.

type. They show Fe_2O_3 between 14.27 and 18.48 wt% with average of 15.04 wt% and Sr variation between 375 and 504 ppm with average 412 ppm. The TiO_2 content varies between 3.21 to 3.97 wt% with average 3.7 wt%, similar to Urubici magma-type, but in the Sr *vs*. TiO_2 diagram the samples plot on the Pitanga field (Tab. 6, Fig. 18).

The two groups of samples identified by major elements are also distinguished by the trace elements (Fig. 17). Negative correlation is observed for incompatible elements Nb, Ba, Ce, Rb and (subtle) Y and Zr. Ni shows defined positive correlation, whereas for Sr there is no clear correlation. Figure 19 reinforces the presence of two groups of basalts and the evidence of two parental magmas in this region. With regard to data from Rocha-Júnior *et al.* (2013), the correspondence observed for the major and minor elements is observed for the trace elements, although it is not so clear for some samples. In addition, all those samples are more Y-enriched than these under analysis.

Only five samples — from the Uberaba and Uberlândia/Araguari regions — were analyzed for Rare Earth Elements
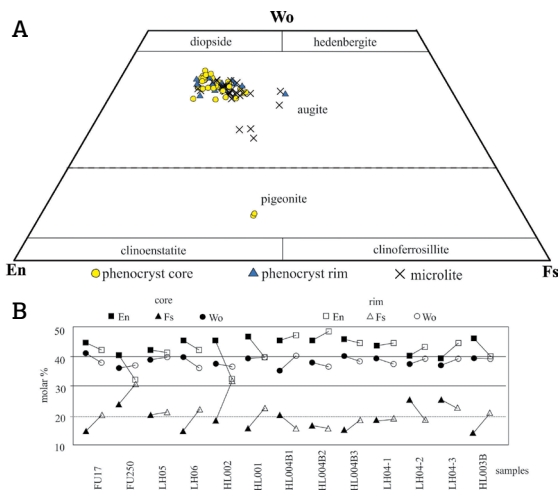
Figure 10. Pyroxene analysis. (A) Compositional variation of pyroxenes according to the ternary diagram (Wo-En-Fs) of Morimoto (1988); (C) compositional variation of pyroxenes according to core-rim profile; cpx crystals HL004B 1, HL004B 2, LH04-2 and LH04-3 show inverted zoning, unlike the others, including the two other crystals analyzed for these same samples (HL004B 3 and LH04-1).

Table 2. Some analysis and formulae of representative pyroxenes.

Sample	FU17 P C	FU17 P R	FU17 MP C	HL001 P C	HL001 P R	HL004c P C	HL004c P C	HL004c MP C	HL004c MP C	LH04 P C	LH04 P R	LH04 MP C
Component												
SiO$_2$	49.430	49.820	47.140	50.120	46.990	49.690	50.540	49.520	50.280	49.520	50.130	50.110
TiO$_2$	1.260	1.150	2.150	1.160	2.640	1.460	1.070	1.440	1.110	1.180	0.960	1.140
Al$_2$O$_3$	2.870	2.090	4.000	2.790	3.980	3.280	2.810	3.100	1.880	3.410	2.810	2.110
Cr$_2$O$_3$	0.260	0.030	0.080	0.000	0.000	0.000	0.000	0.000	0.000	0.000	0.000	0.000
FeOt	9.480	12.410	12.260	9.710	14.010	10.550	10.230	12.280	13.450	11.440	11.630	12.430
MnO	0.230	0.230	0.250	0.230	0.300	0.260	0.240	0.270	0.370	0.270	0.310	0.300
MgO	15.190	14.480	13.500	15.870	12.960	15.000	16.150	14.470	14.70	14.570	14.870	14.460
CaO	19.270	17.660	18.230	18.860	17.890	19.030	18.110	17.600	17.600	18.340	18.030	18.070
Na$_2$O	0.270	0.200	0.300	0.260	0.300	0.240	0.240	0.230	0.200	0.360	0.260	0.230
K$_2$O	0.010	0.030	0.000	0.000	0.000	0.000	0.000	0.000	0.000	0.000	0.000	0.000
Total	98.260	98.100	97.900	99.000	99.070	99.510	99.390	98.910	99.590	99.090	99.000	98.850
Cations based on 6 oxygen												
Si	1.880	0.033	1.824	1.887	1.810	1.870	1.894	1.882	1.908	1.876	1.899	1.910
Ti	0.036	0.094	0.063	0.033	0.077	0.041	0.030	0.041	0.032	0.034	0.027	0.033
Al	0.129	0.001	0.182	0.124	0.181	0.146	0.124	0.139	0.084	0.152	0.126	0.095
Cr	0.008	0.398	0.002	0.000	0.000	0.000	0.000	0.000	0.000	0.000	0.000	0.000
Fe(ii)	0.301	0.007	0.397	0.306	0.451	0.332	0.320	0.390	0.427	0.362	0.368	0.396
Mn	0.007	0.828	0.008	0.007	0.010	0.008	0.008	0.009	0.012	0.009	0.010	0.010
Mg	0.861	0.726	0.778	0.891	0.745	0.842	0.902	0.820	0.832	0.823	0.840	0.821
Ca	0.785	0.015	0.756	0.761	0.739	0.768	0.727	0.717	0.716	0.744	0.732	0.738
Na	0.020	0.001	0.022	0.019	0.022	0.018	0.018	0.017	0.015	0.026	0.019	0.017
K	0.001	0.033	0.000	0.000	0.000	0.000	0.000	0.000	0.000	0.000	0.000	0.000
Cat sum	4.027	4.016	4.032	4.028	4.033	4.024	4.023	4.016	4.025	4.027	4.020	4.019
End-member (%)												
Wo	39.800	36.790	38.590	38.380	37.640	39.060	36.850	36.730	35.820	37.940	37.200	37.260
En	43.650	41.980	39.760	44.960	37.950	42.830	45.730	42.010	41.620	41.930	42.700	41.490
Fs	15.550	20.480	20.520	15.700	23.310	17.210	16.530	20.370	21.810	18.790	19.140	20.400

P: phenocryst; MP: micro-phenocryst; C: core; R: rim.
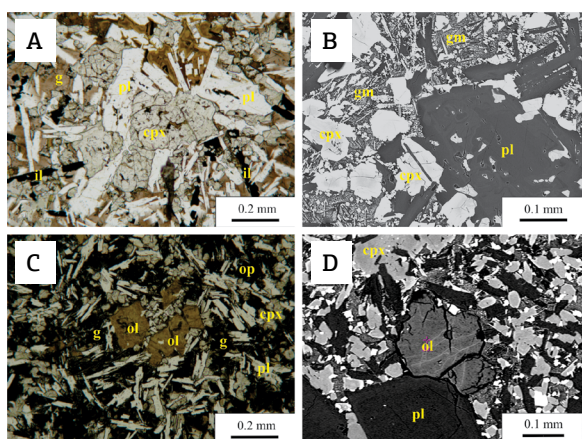
Pl: plagioclase; cpx: clinopyroxene; op: opaque mineral; il: ilmenite; gm: glassy mesostasis; ol: olivine; g: glass.

Figure 11. (A) Crystals of ilmenite between clinopyroxene and plagioclase showing intergranular, intersertal and subophitic textures. Some small plagioclase laths show swallowtail termination. Parallel polarizers; (B) back-scattered image showing some subhedral crystals of ilmenite and abundant skeletal microlites in the mesostasis in process of devitrification; (C) small euhedral crystals of olivine, replaced by iddingsite, together with laths of plagioclase, granular clinopyroxene and oxides. Parallel polarizers; (D) back-scattered image showing some micro-phenocrysts of well-preserved olivine, plagioclase and clinopyroxene, in a mesostasis rich in clinopyroxene and plagioclase apart from oxides and glass.

(REE). The REE were normalized to the chondrites (Sun & McDonough 1989) (Fig. 20) and resemble the data of Rocha-Júnior *et al.* (2013). Heavy REE's are strongly depleted compared to light REE's in the Pitanga magma type. $(La/Lu)_N$ varies between 8.04 to 9.93, while the data from Pitanga magma by Rocha-Júnior *et al.* (2013) are in
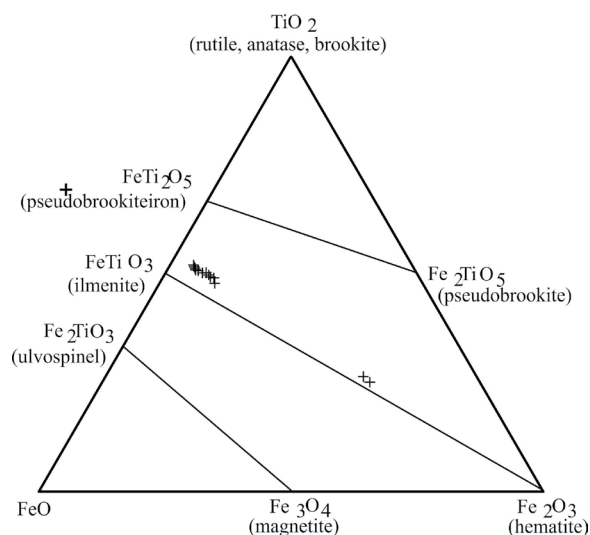

Figure 12. Ternary FeO *vs.* TiO_2 *vs.* Fe_2O_3 diagram (Akimoto and Katsura, 1959) showing the main solid solutions of Fe-Ti oxides. Discussion in text.

Table 3. Analysis and formulae of representative ilmenite.

| Sample	FU17 MP C	FU17 MP C	FU17 MP C	HL012a MP C	HL012a MP C	HL004c MP C	HL004c MP C	HL004c MP C	HL004b MP C	LH05 MP C
Component										
SiO_2	0.010	0.040	0.000	0.020	0.000	0.040	0.050	0.050	0.030	0.290
TiO_2	47.970	47.450	47.860	49.330	48.930	48.280	48.330	47.620	48.780	49.750
Al_2O_3	0.310	0.290	0.280	0.140	0.190	0.240	0.270	0.280	0.150	0.160
FeOt	48.120	48.370	48.340	46.930	47.340	47.810	47.910	47.580	46.970	45.960
MnO	0.440	0.390	0.370	0.460	0.420	0.450	0.440	0.390	0.460	0.480
MgO	1.830	1.530	1.600	1.280	1.310	1.290	1.440	1.350	0.910	1.590
CaO	0.170	0.140	0.070	0.030	0.080	0.120	0.120	0.150	0.000	0.120
Total	98.840	98.170	98.520	98.190	98.270	98.230	98.560	97.420	97.300	98.350
Cations based on 4 oxygen										
Si	0.000	0.002	0.000	0.001	0.000	0.002	0.003	0.003	0.002	0.015
Ti	1.862	1.859	1.867	1.918	1.905	1.886	1.880	1.876	1.919	1.918
Al	0.019	0.018	0.017	0.008	0.011	0.015	0.018	0.017	0.009	0.010
Fe(ii)	2.076	2.107	2.096	2.029	2.049	2.076	2.071	2.084	2.054	1.970
Mn	0.019	0.017	0.016	0.020	0.019	0.020	0.019	0.017	0.020	0.021
Mg	0.141	0.119	0.124	0.099	0.101	0.100	0.111	0.106	0.071	0.122
Ca	0.009	0.008	0.004	0.002	0.005	0.006	0.007	0.009	0.000	0.007
Cat sum	4.127	4.130	4.124	4.077	4.089	4.105	4.109	4.112	4.075	4.062

MP: micro-phenocryst; C: core.

the 6.1 to 10.3 range. Eu shows a very slightly negative anomaly with Eu/Eu* values of 0.92 to 0.94.

Table 4. Representative analysis and formulae of olivine.

Sample	FU 17 P C	FU 17 P C	FU 250 MP C	FU 250 MP C
Component				
SiO_2	34.840	34.890	31.570	31.730
TiO_2	0.070	0.080	0.260	0.120
Al_2O_3	0.040	0.050	0.020	0.000
FeO_t	33.960	34.010	54.020	53.410
CaO	0.330	0.390	0.380	0.350
MnO	0.450	0.480	0.920	0.830
MgO	28.270	27.960	12.230	12.690
NiO	0.060	0.070	0.010	0.000
Total	98.020	97.930	99.420	99.147
Cations based on 4 oxygen				
Si	0.990	0.993	0.988	0.992
Ti	0.002	0.002	0.006	0.003
Al	0.001	0.002	0.001	0.000
Fe(ii)	0.807	0.809	1.414	1.396
Mn	0.011	0.012	0.024	0.022
Mg	1.197	1.186	0.571	0.592
Ni	0.001	0.002	0.000	0.000
Ca	0.010	0.012	0.013	0.012
Cat sum	3.019	3.018	3.017	3.017
End-member (%)				
Fo	59.430	59.107	28.407	29.434

P: phenocryst; MP: micro-phenocryst; C: core.
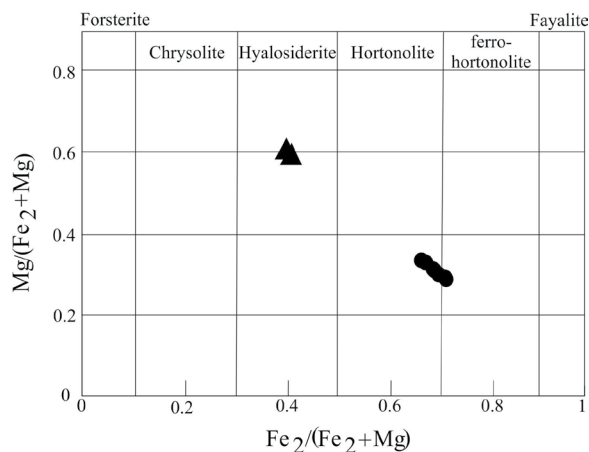

Source: modified from Sarmento et al. (2017).

Figure 13. Compositional variation of olivine from samples FU017 (full triangle), FU250 and LH05 (full circle).

The multi-elemental distribution patterns normalized to primitive mantle show negative Nb anomalies, also observed for all high- and low-Ti tholeiites of the PCMP. The $(Rb/Ba)_{PM}$ ratios < 1 (varying from X to Y) is an indicative that the investigated basalt flows were not affected by low-pressure crustal contamination processes (*e.g.*, Peate 1997, Marques *et al.* 1999, Marques *et al.* 2017).

DISCUSSION

In the Lower Cretaceous, the north and northeast edge of the Paraná Basin was delimited by topographically elevated terrains, known as Alto Paranaíba Arch, whose palaeorelief was highly irregular. These peculiarities determined the design and characteristics of the sedimentary and volcanic deposits. In such peridesertic region, occasional aqueous flows generated alluvial fan deposits and/or fluvio-lacustrine systems and, in addition, allowed the occurrence of pillow lavas. These characteristics — together with the broad domain of entablature on colonnades, very fine textured basalts, mesostasis with significant amount of glass and fossil records in contemporaneous sediments — are indicative of a more humid environment than the dominant in the rest of the PCMP. On the other hand, the predominance of intertrapped aeolian sandstone lenses in thin basalt flows suggests irregular topography and peripheral location.

Under microscopy, thin sections of entablature show abundant microlites and frequent plagioclase with swallow-tail-like texture, opaque minerals with skeletal texture and volcanic glass in mesostasis. These characteristics are less frequent in thin-sections of colonnade samples, indicating a less quick cooling rate for the last one.
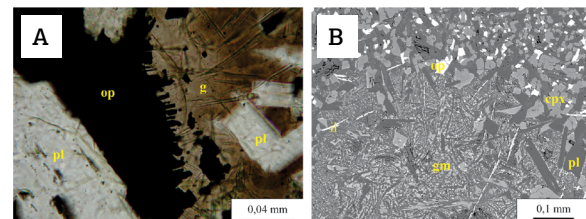
Pl: plagioclase; cpx: clinopyroxene; op: opaque mineral; il: ilmenite; gm: glassy mesostasis; g: glass.

Figure 14. (A) Typical example of vitreous mesostasis in the devitrification process; crystallites of clinopyroxene and plagioclase in plumose texture are abundant and associated with skeletal oxide crystals; (B) back-scattered image showing mesostasis with crystalites of plagioclase, pyroxene and opaque minerals.

Table 5. Whole-rock analysis of 22 basalt samples and CIPW Norm data.

Sample	HL001	HL003A	HL003D	HL004C	HL004E	HL004J*	HL011B*	HL011C	HL013A*	HL013B	HLA1
Long (-)	47.6235	48.2108	48.2108	48.2136	48.2136	48.2136	48.3241	48.3241	48.3240	48.3240	48.2240
Lat (-)	19.2819	18.7259	18.7259	12.8183	12.8183	12.8183	18.8754	18.8754	18.8863	18.8863	18.7289
Major elements (wt. %)											
SiO_2	49.7600	47.6100	49.5800	49.7500	47.7100	49.9300	50.5300	49.8000	50.9000	49.7300	47.5900
TiO_2	3.2100	3.3700	3.2400	3.5400	3.5600	3.6100	3.5800	3.5600	3.7100	3.5200	3.5700
Al_2O_3	12.6200	11.9800	12.6600	12.5000	12.6700	12.5300	12.5900	12.4800	12.7500	12.3600	12.5000
$Fe_2O_3(t)$	14.2900	18.4800	14.2700	14.6200	14.7700	14.8400	14.3300	14.7800	14.5200	14.7400	15.3100
CaO	9.7700	8.8600	9.8400	9.2900	9.6600	9.4000	9.8500	9.3600	9.6200	9.2900	9.0000
MgO	5.4300	4.6100	5.3300	4.8200	4.9300	4.7200	4.8200	4.7700	5.0300	4.8000	4.8000
Na_2O	2.4700	2.7800	2.6600	2.8700	2.3500	2.8800	2.8900	2.8200	2.8600	2.8300	2.6400
K_2O	0.9900	0.7700	0.8000	0.8400	1.4900	0.8500	0.8200	0.9300	0.8900	0.9000	1.3000
P_2O_5	0.3600	0.4200	0.3700	0.4400	0.4300	0.4300	0.4700	0.4500	0.4300	0.4400	0.4500
MnO	0.1900	0.2400	0.1800	0.2000	0.1800	0.2000	0.2200	0.1900	0.2200	0.1800	0.2100
LOI	0.8800	1.0100	1.0400	1.1100	2.2400	1.1500	0.9900	0.9500	0.9000	1.2200	2.6300
Total	99.9700	100.1300	99.9700	99.9800	99.9900	100.5400	100.0900	100.0900	101.8300	100.0100	100.0000
CIPW Norm (%)											
qz	0.0000	0.0000	1.3900	1.8200	0.0000	1.2100	2.1200	1.7400	2.1300	1.8100	0.0000
or	9.7600	4.8000	4.9000	5.2000	9.3500	5.2000	5.0000	5.7500	5.3500	5.6000	8.2000
ab	23.1000	26.1000	24.8500	26.9500	22.3500	26.8500	26.7000	26.3500	26.2500	26.5000	25.2000
an	21.2000	18.7800	21.0500	19.5000	20.6800	18.8800	19.5300	19.4300	19.7300	19.2000	19.4800
di	21.3200	19.4800	21.6800	22.8800	21.6000	23.2000	22.1200	20.6800	20.9200	20.7600	19.8400
en	10.8400	18.1600	18.4600	15.3800	16.1600	16.4000	16.3800	17.8000	17.4200	17.9400	16.3800
ol	6.2700	3.8700	0.0000	0.0000	1.5300	0.0000	0.0000	0.0000	0.0000	0.0000	2.4000
mt	2.0300	2.6400	2.0300	2.7800	2.1300	2.1000	2.0100	2.1000	2.0300	2.1000	2.2200
il	4.6600	4.9200	4.7000	5.1400	5.2600	5.2200	5.1400	5.1800	5.2800	5.1400	5.2800
ap	0.8000	0.9300	0.8300	0.9500	0.9600	0.9400	1.0100	0.9900	0.9300	0.9600	1.0100
total	99.9800	99.6800	99.8900	100.6000	100.0200	100.0000	100.0100	100.0200	100.0400	100.0100	100.0100
Trace elements (ppm)											
Zn	104.0000	107.0000	103.0000	108.0000	105.0000	117.0000	112.0000	107.0000	113.0000	101.0000	116.0000
Cu	168.0000	163.0000	180.0000	164.0000	171.0000	185.0000	188.0000	161.0000	186.0000	162.0000	99.0000
Cr	134.0000	57.0000	121.0000	69.0000	59.0000	-	-	68.0000	57.0000	57.0000	12.0000
Ni	66.0000	53.0000	66.0000	60.0000	51.0000	59.0000	64.0000	53.0000	60.0000	50.0000	22.0000
Ba	340.0000	402.0000	347.0000	422.0000	412.0000	490.0000	396.0000	426.0000	394.0000	435.0000	498.0000
Co	37.0000	38.0000	39.0000	41.0000	38.0000	39.2000	39.6000	41.0000	38.5000	39.0000	38.0000
Cs	-	-	-	0.3200	-	0.3300	0.2500	-	0.2600	-	-
Ga	20.0000	20.0000	20.0000	22.5000	20.0000	22.4000	22.6000	20.0000	22.8000	21.0000	19.0000
Hf	-	-	-	6.2400	-	6.0800	5.8400	-	5.8700	-	-
Nb	20.0000	20.0000	19.0000	22.3600	19.0000	20.9100	21.7100	20.0000	20.1200	20.1200	22.0000
Rb	23.0000	20.0000	20.0000	20.1000	28.0000	23.0000	22.9000	21.0000	21.7000	20.0000	18.0000
Sn	-	-	-	1.5000	-	1.1000	0.9000	-	0.9000	-	-
Sr	375.0000	380.0000	388.0000	381.1000	403.0000	480.0000	491.0000	377.0000	488.0000	377.0000	405.0000
Th	-	-	-	4.8000	-	3.8000	3.2000	-	3.1000	-	-
U	-	-	-	0.7100	-	0.6900	0.7800	-	0.6400	-	-

Table 5. Continuation.

Sample	HL001	HL003A	HL003D	HL004C	HL004E	HL004J*	HL011B*	HL011C	HL013A*	HL013B	HLA1
Long (-)	47.6235	48.2108	48.2108	48.2136	48.2136	48.2136	48.3241	48.3241	48.3240	48.3240	48.2240
Lat (-)	19.2819	18.7259	18.7259	12.8183	12.8183	12.8183	18.8754	18.8754	18.8863	18.8863	18.7289
Major elements (wt. %)											
Zr	175.0000	197.0000	176.0000	198.0000	191.0000	229.0000	242.0000	196.0000	246.0000	198.000	230.000
Y	27.0000	29.0000	26.0000	30.9700	29.0000	29.9100	32.0100	29.0000	30.6100	29.000	31.0000
La	12.0000	25.0000	25.0000	32.5000	29.0000	30.3000	40.3000	24.0000	33.9000	31.000	30.0000
Ce	74.0000	73.0000	66.0000	81.0000	73.0000	67.5000	74.3000	67.0000	68.8000	73.000	83.0000
Pr	-	-	-	8.7900	-	8.6600	9.2900	-	8.7000	-	-
Nd	-	-	-	37.4000	-	37.2000	39.6000	-	37.9000	-	-
Sm	-	-	-	8.1000	-	8.2000	8.5000	-	8.2000	-	-
Eu	-	-	-	2.5300	-	2.5300	2.6100	-	2.5100	-	-
Gd	-	-	-	8.2200	-	8.0400	8.4500	-	8.1200	-	-
Tb	-	-	-	1.2000	-	1.1900	1.2500	-	1.1800	-	-
Dy	-	-	-	6.6400	-	6.5600	6.8200	-	6.6000	-	-
Ho	-	-	-	1.2600	-	1.2500	1.2900	-	1.2500	-	-
Er	-	-	-	3.4600	-	3.3300	3.5500	-	3.3800	-	-
Tm	-	-	-	0.4800	-	0.4600	0.4600	-	0.4400	-	-
Yb	-	-	-	2.8000	-	2.7000	2.8000	-	2.7000	-	-
Lu	-	-	-	0.4100	-	0.3900	0.4200	-	0.3900	-	-

Sample	HLA7	FU17*	FS065	FS066	FS129	FS229	FS236	FS252	LH03	LH04	LH05
Long (-)	48.2264	47.9590	47.4383	47.4529	47.4402	47.3380	47.3674	47.4322	48.2191	48.2192	48.2193
Lat (-)	18.7118	19.9550	19.6112	19.6050	19.9639	19.7701	19.7733	19.8493	18.7262	18.7261	18.7260
Major elements (wt. %)											
SiO_2	49.7100	50.1200	50.5300	50.6800	49.9300	51.4200	50.8900	50.4800	46.7300	50.7000	49.3200
TiO_2	3.2300	3.5400	3.8800	3.9000	3.9700	3.6400	3.6300	3.9100	3.5900	3.4600	3.2500
Al_2O_3	12.6700	12.5400	11.8700	11.9400	12.6300	12.1600	12.2100	11.8500	12.6100	12.1100	12.5700
$Fe_2O_3(t)$	14.4200	14.6800	15.8500	14.9400	14.5000	15.0100	15.2800	15.7300	15.6800	15.0200	14.7700
CaO	9.8000	9.4000	8.0400	8.2200	8.1400	8.0700	8.1800	8.0300	9.2500	8.3300	9.7900
MgO	5.4900	4.4600	3.9200	4.1200	4.3500	4.0300	4.1800	3.9400	5.0200	3.9300	5.4700
Na_2O	2.5700	2.6900	2.6300	2.8300	3.0000	2.6800	2.7800	2.6300	2.4900	3.0100	2.5300
K_2O	0.9400	1.0400	1.6400	1.4900	1.4900	1.5200	1.4900	1.5300	1.0600	1.1700	1.1700
P_2O_5	0.3600	0.4400	0.6600	0.7900	0.6500	0.5100	0.5100	0.6600	0.4600	0.4500	0.3700
MnO	0.1800	0.2100	0.2200	0.2000	0.2000	0.2000	0.2000	0.2200	0.2200	0.1900	0.1900
LOI	0.6400	0.1500	0.9500	0.9200	1.1300	0.7400	0.6600	0.9800	2.9000	1.5800	0.8200
Total	100.0100	99.2700	100.1900	100.0300	99.9900	99.9800	100.0100	99.9600	100.0100	99.9500	99.9800
CIPW Norm (%)											
qz	0.5200	2.2600	4.0200	2.0600	1.2300	4.6700	3.3400	1.9200	0.0000	3.1900	0.9000
or	5.8000	6.4000	9.7000	9.2500	9.200	9.4000	9.1500	9.5500	6.6500	7.3000	5.5500
ab	23.9000	25.1000	22.1000	26.6000	27.8200	25.2500	26.0000	24.8500	23.8500	28.4500	23.6000
an	20.9500	19.8000	16.4000	16.1500	17.3000	17.3500	17.1800	16.8300	21.4000	16.9000	21.0800
di	23.5200	20.5200	17.3300	21.2400	19.9200	16.8000	17.3200	18.2600	19.4000	18.8800	21.4000
en	18.3400	17.7800	19.1000	16.8800	16.1600	17.9800	18.4200	18.6400	17.2000	17.1000	19.8400

Table 5. Continuation.

Sample	HLA7	FU17*	FS065	FS066	FS129	FS229	FS236	FS252	LH03	LH04	LH05
Long (-)	48.2264	47.9590	47.4383	47.4529	47.4402	47.3380	47.3674	47.4322	48.2191	48.2192	48.2193
Lat (-)	18.7118	19.9550	19.6112	19.6050	19.9639	19.7701	19.7733	19.8493	18.7262	18.7261	18.7260
ol	0.0000	0.0000	0.0000	0.0000	0.0000	0.0000	0.0000	0.0000	2.8500	0.0000	0.0000
mt	2.0400	2.0700	2.9100	0.0500	2.0600	2.1500	2.1800	2.2500	2.2800	2.1500	2.0900
il	4.6200	5.1200	6.4300	5.6800	5.7800	5.3000	5.2200	5.7200	5.3400	5.0800	4.7200
ap	0.8000	0.9600	2.0000	1.7500	1.4200	1.1200	1.1200	1.4400	1.0400	0.9600	0.8300
Total	100.4900	100.0100	99.9900	99.6600	100.8900	100.0200	99.9300	99.4600	100.0100	100.0100	100.0100
Trace elements (ppm)											
Zn	98.0000	118.0000	139.0000	125.0000	125.0000	120.0000	109.0000	121.0000	114.0000	105.0000	98.0000
Cu	179.0000	188.0000	136.0000	60.0000	85.0000	63.0000	58.0000	138.0000	88.0000	119.0000	176.0000
Cr	126.0000		18.0000	6.0000	30.0000	17.0000	15.0000	10.0000	16.0000	9.0000	116.0000
Ni	66.0000	62.0000	20.0000	21.0000	43.0000	21.0000	20.0000	23.0000	20.0000	22.0000	64.0000
Ba	383.0000	458.0000	517.0000	528.0000	583.0000	500.0000	501.0000	497.0000	458.0000	539.0000	368.0000
Co	42.0000	40.3000	38.00000	38.0000	39.0000	38.0000	35.0000	34.0000	42.0000	38.0000	38.0000
Cs	-	0.2700	-	-	-	-	-	-	-	-	-
Ga	20.0000	22.4000	20.0000	20.0000	21.0000	21.0000	21.0000	21.0000	20.0000	21.0000	19.0000
Hf	-	5.7800	-	-	-	-	-	-	-	-	-
Nb	19.0000	19.6400	27.00000	25.0000	26.0000	22.0000	21.0000	28.0000	22.0000	21.0000	17.0000
Rb	21.0000	18.5000	32.00000	29.0000	30.0000	28.0000	26.0000	31.0000	14.0000	21.0000	21.0000
Sn	-	0.9000	-	-	-	-	-	-	-	-	-
Sr	376.0000	475.0000	394.0000	471.0000	504.0000	378.0000	382.0000	386.0000	392.0000	393.0000	377.0000
Th	-	2.9000	-	-	-	-	-	-	-	-	-
U	-	0.6400	-	-	-	-	-	-	-	-	-
V	423.0000	481.0000	397.00000	319.0000	417.0000	407.0000	390.0000	400.0000	464.0000	418.0000	421.0000
W	-	1.4000	-	-	-	-	-	-	-	-	-
Zr	175.00000	243.0000	243.0000	230.0000	234.0000	225.0000	225.0000	244.0000	228.0000	228.0000	171.0000
Y	27.0000	30.3500	33.0000	32.0000	30.0000	31.0000	32.0000	32.0000	30.0000	31.0000	27.0000
La	22.0000	32.2000	23.0000	35.0000	22.0000	23.0000	23.0000	27.0000	33.0000	31.0000	18.0000
Ce	65.0000	67.9000	93.0000	98.0000	94.0000	95.0000	83.0000	114.0000	94.0000	91.0000	74.0000
Pr	-	8.7300	-	-	-	-	-	-	-	-	-
Nd	-	37.2000	-	-	-	-	-	-	-	-	-
Sm	-	8.3000	-	-	-	-	-	-	-	-	-
Eu	-	2.4900	-	-	-	-	-	-	-	-	-
Gd	-	7.9800	-	-	-	-	-	-	-	-	-
Tb	-	1.1600	-	-	-	-	-	-	-	-	-
Dy	-	6.6700	-	-	-	-	-	-	-	-	-
Ho	-	1.2600	-	-	-	-	-	-	-	-	-
Er	-	3.3000	-	-	-	-	-	-	-	-	-
Tm	-	0.4500	-	-	-	-	-	-	-	-	-
Yb	-	2.7000	-	-	-	-	-	-	-	-	-
Lu	-	0.4000	-	-	-	-	-	-	-	-	-

Source: Fujimori, 1990; HL and LH: Uberlândia/Araguari region; FU: Uberaba region; FS: Sacramento region; qz: quartz; or: orthoclase; ab: albite; an: anorthite; di: diopside; en: enstatite; ol: olivine; mt: magnetite; il: ilmenite; ap: apatite; *analyzed by Geosol.
Trace and rare earth elements from HL004C were determined by Geosol. See text for details.
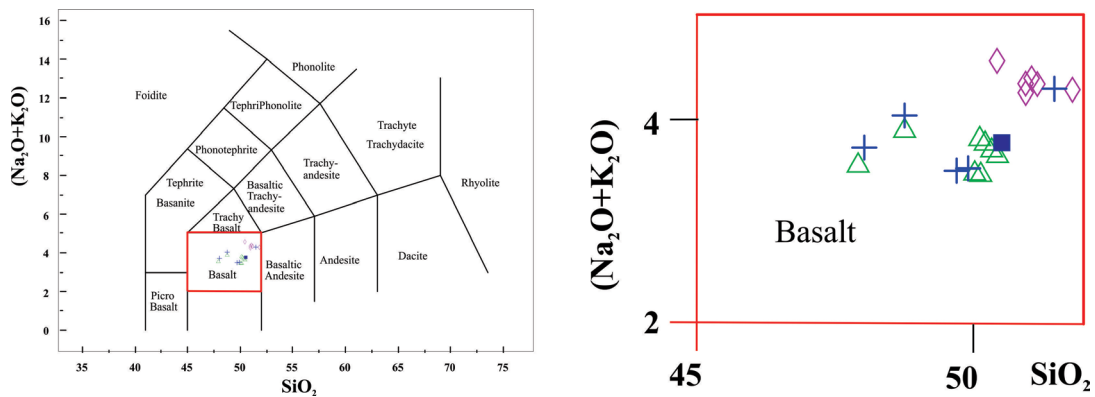
Empty diamonds: Sacramento; full square: Uberaba; empty triangles: Uberlândia/Araguari and crosses: basalt flows related to pillow lavas.

Figure 15. Classification and chemical nomenclature of the studied samples. Total alkali-versus-silica (TAS) diagram (alkalis *vs*. SiO$_2$), according to Le Bas *et al*. (1986).
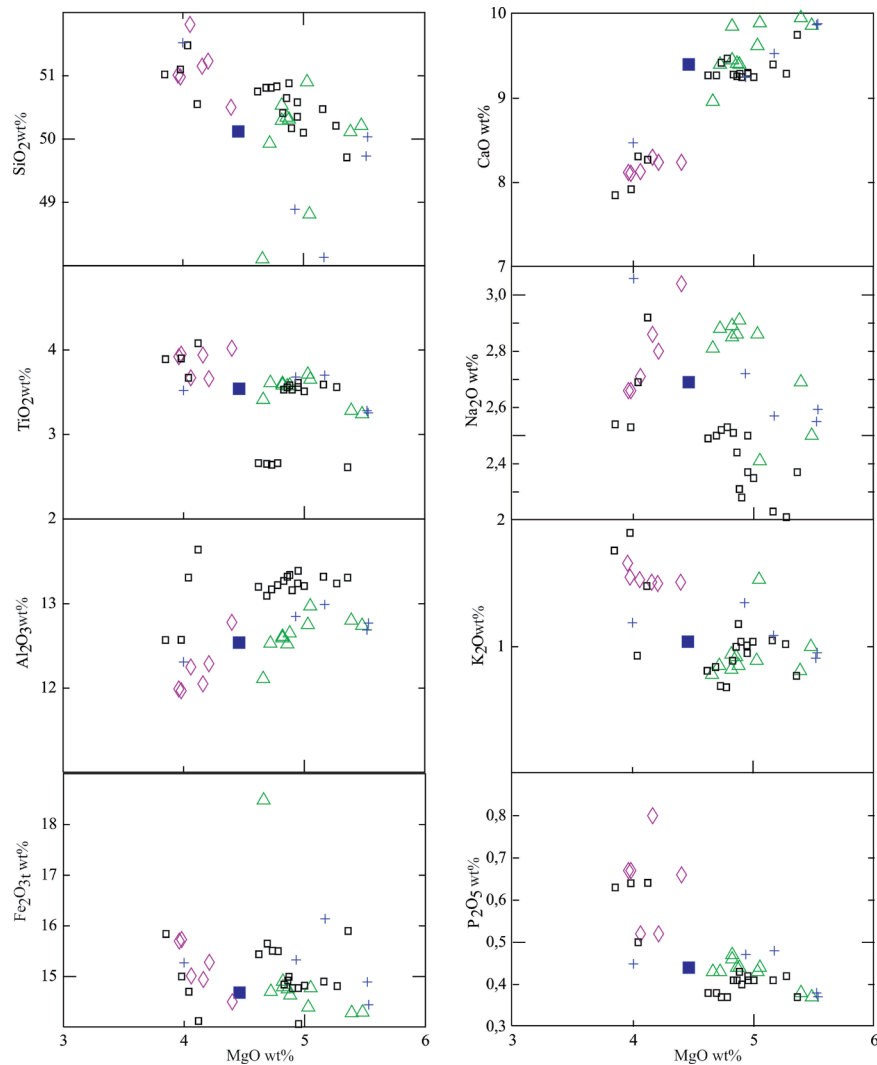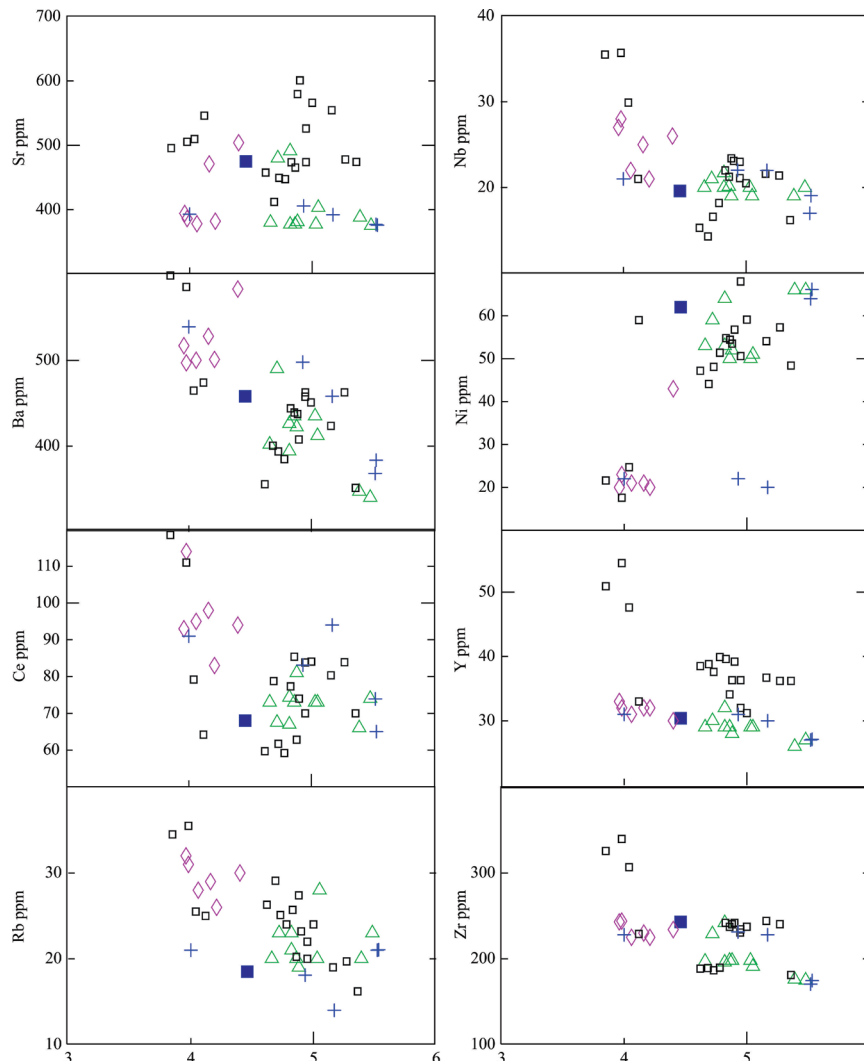

Empty squares: 18 samples from the Triângulo Mineiro and northeast of São Paulo (Rocha Junior *et al.*, 2013); empty diamonds: Sacramento; full square: Uberaba; empty triangles: Uberlândia/Araguari and crosses: basalt flows related to pillow lavas).

Figure 16. Diagrams for major and minor elements *vs*. MgO.

An unusual feature is the presence of inverted or alternating zoning from the core to the edge in some plagioclase and pyroxene crystals. According to Vernon (2004, p. 139-141), even though it has been produced in the laboratory, reverse discontinuous zoning is uncommon in igneous rocks. However, it could be produced by a rapidly induced temperature variation (caused by, for example, rapid movement of magma in a chamber, volcanic eruption, rapid release of volatiles in a water-saturated magma, or magma mixing). This author also discusses patchy zoning which, as stated by Vance (1965 *apud* Vernon 2004), is due to initial crystallization of relatively calcic plagioclase in a water-undersaturated magma at depth, that suffer a rapid decrease in confining pressure, causing resorption. A new crystallization of more sodic plagioclase begins to fill cavities in the nuclei — forming pseudoinclusions — and enveloping it with a composition different from that of the previous zones. Not rarely, small inclusions (*e.g.*, of glass or pyroxene) occur in the more sodium-rich patches, generated from trapped melt in the corroded core. Normal and reverse oscillatory zoning may also occur in clinopyroxene — generally oscillating between augite and subcalcic augite, — and is explained as the response to local diffusion limitations, as in the case of plagioclase. It should also be recorded that two pigeonitic cores were identified in pyroxene phenocrysts.

Still with respect to plagioclases, the overlaps between the compositions of groundmass and phenocrysts, illustrated in the ternary classification diagram Ab–An–Or (Fig. 7), suggest the simultaneous crystallization of both phenocrysts edges and groundmass (Rao *et al.* 2012).

Empty squares: 18 samples from the Triângulo Mineiro and northeast of São Paulo (Rocha Junior *et al.*, 2013); empty diamonds: Sacramento; fullsquare: Uberaba; empty triangles: Uberlândia/Araguari and crosses: basalt flows related to pillow lavas).

Figure 17. Diagrams for trace elements *vs*. MgO.

Olivines, with hyalosiderite (Fo59), hortonolite and fer-rohortonolite (Fo28) composition, were identified in samples from Uberaba and Uberlândia/Araguari regions. The current level of knowledge does not permit discussing the relationships/meaning between the basaltic flows with these distinct olivines. However, the data are in agreement with ones presented by Machado (2009) for magmas of the Pitanga type, in the northwest of the Province. This kind of record is present in olivine phenocrysts of lava flows from Linga area of the Eastern Deccan Volcanic Province. According to Ganguly *et al.* (2012), while the high iron content denotes a magma with much-evolved composition, the broad compositional spectrum of phenocrysts corroborates a changing crystallization condition in the predominant magmatic environment. More detailed studies are needed to test this hypothesis for Pitanga magma type.

These rocks are classified as basalts and have a tholeiitic character, with strong enrichment of iron in relation to alkalis and magnesium. Although the TiO_2 content shows 3.7 wt% in average, similar to Urubici magma type, the samples plot on the Pitanga field in the Sr *vs.* TiO_2 diagram. Two specific fields are clear in major oxides / trace elements *vs.* MgO diagrams: one for less evolved rocks (MgO > 4.65 wt%) from the Uberlândia/Araguari region; and other one for those more evolved rocks from the Sacramento region (MgO < 4.35 wt%), with the single sample of the Uberaba region in the intermediate area, between the two groups. Samples of the basalt flows related to pillow lavas plot scattered among the groups mentioned. Sample HL04, however, shows an enrichment in SiO_2, Na_2O and Rb, and impoverishment in CaO and MgO, which suggests alteration by water interaction. In general, there is a correspondence with Rocha-Júnior *et al.* (2013) data, although these exhibit lower values for Na_2O and higher for Al_2O_3, suggesting the possibility of some analytical bias.

Heavy REE are depleted compared to light rare-earth elements (*LREE*) with $(La/Lu)_N$ between 8.04 to 9.93, and, although some enrichment in LREE is expected as a result of fractional crystallization, the high $(La/Lu)_N$ values are indicative of partial melting of a garnet peridotite, constraining the mantle source to depths greater than 80 km (Wilson 2007). Taking into account that $(Rb/Ba)_{PM}$ ratios are < 1 in all analyzed basalts, suggesting that the magmas did not suffer crustal contamination during their ascension to surface, the Nb negative anomaly observed in the multi-elemental trace element patterns is a mantle source feature. According to Rocha-Júnior *et al.* (2012, 2013) the sources of PCMP basalts were affected by Neoproterozoic subductions (generating the depletion in Nb) related with the Gondwana Assembly.

The trends observed for major, minor and trace elements in the variation diagrams (Figs. 16 and 17) are broadly compatible with fractional crystallization of clinopyroxene, plagioclase and Ti-magnetite. The slightly negative Eu anomalies (Eu/Eu*= 0.92 – 0.94) in the REE distribution patterns reinforce plagioclase fractionation. Besides that, the geochemical data point to evolution involving at least two parental magmas, as evidenced by their distinct Ba/Zr, Nb/Zr and Nb/Y ratios (Fig. 19). One of them would generate the basalts of Sacramento, whereas the other one originated the Araguari/Uberlândia, Uberaba and Perdizes tholeiite group. It is noteworthy that the last group presents some variation in major, minor and trace elements, such as TiO_2, P_2O_5, Rb/Sr, Zr/Nb, which is also suggestive of different parental magmas, but additional highly incompatible trace element data are necessary to corroborate this possibility.

CONCLUDING REMARKS

The northeast edge of the South American portion of the PEP is formed by heterogeneous lava packages with

Table 6. Classification of the basaltic rocks from the studied area according to Peate *et al.* (1992) parameters.

Sample	TiO_2	Sr ppm	Ti/Y	Zr/Y	Magma type
HL001	3.24	375	740	6.48	Pitanga
HL003A	3.41	380	703	6.79	Pitanga
HL003D	3.28	388	753	6.77	Pitanga
HL004C	3.58	381	764	7.07	Pitanga
HL004E	3.65	403	689	6.59	Pitanga
HL004J	3.61	480	722	7.66	Pitanga
HL0011B	3.58	377	668	7.56	Pitanga
HL0011C	3.60	377	741	6.76	Pitanga
HL0013A	3.71	488	725	8.04	Pitanga
HL0013B	3.57	377	738	6.83	Pitanga
HLA1	3.67	405	645	7.42	Pitanga
HLA7	3.25	376	741	6,48	Pitanga
FU17	3,54	475	698	8.01	Pitanga
FS 065	3.88	394	703	7.36	Pitanga
FS 066	3.90	471	731	7.19	Pitanga
FS 129	3.97	504	793	7.8	Pitanga
FS 229	3.64	378	703	7.26	Pitanga
FS 236	3.64	382	681	7.03	Pitanga
FS 252	3.91	386	732	7.60	Pitanga
LH03	3.59	392	716	7.60	Pitanga
LH04	3.46	393	647	7.13	Pitanga
LH05	3.25	377	722	6.33	Pitanga
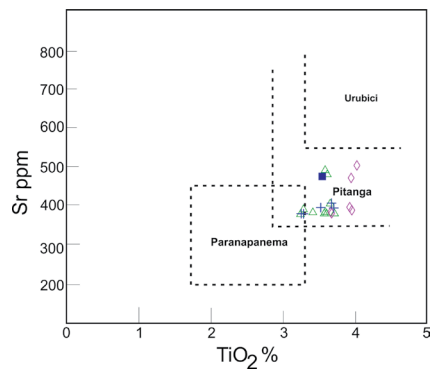
Empty squares: 18 samples from the Triângulo Mineiro and northeast of São Paulo (Rocha Junior et al., 2013); empty diamonds: Sacramento; full square: Uberaba; empty triangles: Uberlândia/Araguari and crosses: basalt flows related to pillow lavas).

Figure 18. Sr *vs*. TiO$_2$ diagram for high titanium magma-types based in Peate *et al.* (1992) and Machado (2005).
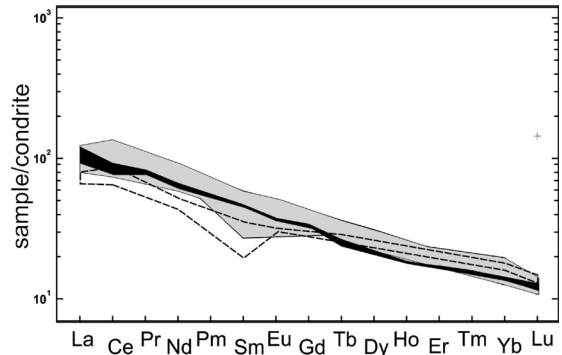

Figure 20. Chondrite-normalized rare Earth elements (REE) (black field) compared with Rocha Junior *et al.* (2013) data (gray field = Pitanga Magma; empty field = Paranapanema Magma).
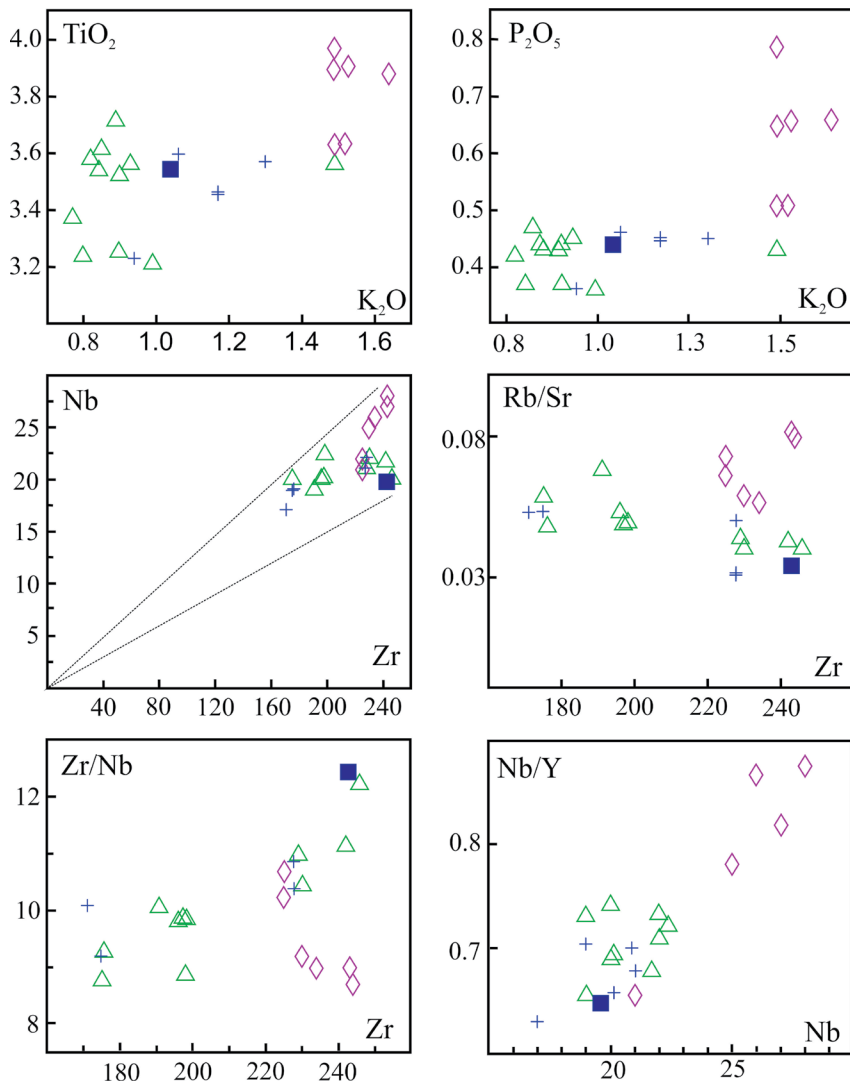
Figure 19. Diagrams variation in some major, minor and trace elements suggestive of different parental magmas.

distinct morphology and chemistry. The rocks are basalts, with a tholeiitic signature, belong to the Serra Geral Group and are classified as Pitanga magma-type, of the high titanium group of basalts. The intertrapped sedimentary beds, aeolian or lacustrine in character, are important markers on prevailing environmental conditions, as well as quiescence periods in the volcanic activity.

Some zoned plagioclase and pyroxene crystals show inverted or alternating zoning from the core to the edge, which could indicate rapidly temperature variation. Still with respect to plagioclases, the ternary classification diagram Ab–An–Or shows overlaps between groundmass and phenocrysts compositions, suggesting simultaneous crystallization of them.

A pronounced chemical distinction can be seen between the rocks from the Uberlândia/Araguari region and those from the Sacramento region, which are more evolved than the first one. Attention is drawn to the independent behavior of rocks associated with pillow lavas, suggesting a possible alteration by water interaction. The origin of these magmas may be to the partial melting of a garnet peridotite mantle source, and the negative anomaly of Nb may be an inheritance of the subduction processes that affected the region during the Neoproterozoic.

The data presented reinforce the need for a more detailed lithostratigraphic control in order to advance the understanding of the processes that acted in the origin of this region of PCMP.

ACKNOWLEDGMENTS

REFERENCES

Akimoto S.I., Katsura T. 1959. Magneto-chemical study of the generalized titanomagnetite in volcanic rocks. *Journal of Geomagnetism and Geoelectricity*, **10**(3):69-90.

Araujo J.S. 1982. *Estruturas Circulares de Água Vermelha.* Dissertation, Instituto de Geociências da Universidade de São Paulo, São Paulo, São Paulo.

Barcelos J.H. 1989. Influência do soerguimento do Alto Paranaíba na sedimentação pós basáltica na área do Triângulo Mineiro (MG), borda NNE da Bacia do Paraná. *Geociências*, **8**:37-54.

Batezelli A. 2003. *Análise da sedimentação cretácea no Triângulo Mineiro e sua correlação com áreas adjacentes.* PhD Thesis, Universidade Estadual Paulista "Júlio de Mesquita Filho", Rio Claro, São Paulo.

Bellieni G., Comin-Chiaramonti P., Marques L.S., Martinez L.A., Melfi A.J., Nardy A.J.R., Papatrechas C., Piccirillo E.M., Roisenberg A., Stolfa D. 1986. Petrogenetic aspects of acid and basaltic lavas from the Paraná Plateau (Brazil): geological, mineralogical and petrochemical relationships. *Journal of Petrology*, **27**:915-944.

Bellieni G., Comin-Chiaramonti P., Marques L.S., Melfi A.J., Piccirillo E.M., Nardy A.J.R., Roisenberg A. 1984. High- and low-Ti flood basalts from the Paraná plateau (Brazil): petrology and geochemical aspects bearing on their mantle origin. *Neues Jahrbuch* für Mineralogie, **150**:273-306.

Deer W.A., Howie R.A., Zussman J. 2003. *An Introduction to the Rock-Forming Minerals.* New York, Longman Scientific and Technical.

Ernesto M., Raposo M.I.B., Marques L.S., Renne P.R., Diogo L.A., De Min A. 1999. Paleomagnetism, geochemistry and 40Ar/39Ar dating of the North-eastern Paraná Magmatic Province: tectonic implications. *Journal of Geodynamics*, **28**:321-340.

Ernesto M., Marques L.S., Piccirillo E.M., Molina E.C., Ussami N., Comin-Chiaramonti P., Bellieni G. 2002. Paraná Magmatic Province-Tristan da Cunha plume system: fixed versus mobile plume, petrogenetic considerations and alternative heat sources. *Journal of Volcanology and Geothermal Research*, **118**:15-36.

Ferreira C.M. 1985. Ocorrência de "*pillow lava*" em vulcanitos da Formação Serra Geral em Araguari, MG. *In*: 3º Simpósio de Geologia de Minas Gerais. *Anais*. Sociedade Brasileira de Geologia, Belo Horizonte, p. 235-237.

Fujimori S. 1990. *Composição química de rochas e suas aplicações.* Salvador, Centro Editorial e Didático da UFBA.

Ganguly S., Ray J., Koeberl C., Ntaflos T., Banerjee M. 2012. Mineral chemistry of lava flows from Linga area of the Eastern Deccan Volcanic Province, India. *Journal of Earth System Science*, **121**(1):91-108.

Hasui Y. 1967. *Geologia das formações cretáceas do Oeste de Minas Gerais.* PhD Thesis, DEM Escola Politécnica, Universidade de São Paulo, São Paulo, São Paulo.

Hooper P.R. 2000. Chemical discrimination of Columbia River basalt flows. *Geochemistry, Geophysics, Geosystems*, **1**(6):1-14. http://dx.doi.org/10.1029/2000GC000040

Irvine T.N., Baragar W.R.A. 1971. A guide to the chemical classification of the common volcanic rocks. *Canadian Journal of Earth Sciences*, **8**(5):523-548.

Janasi V.A., de Freitas V.A., Heaman L.H. 2011. The onset of flood basalt volcanism, Northern Paraná Basin, Brazil: A precise U–Pb baddeleyite/zircon age for a Chapecó-type dacite. *Earth and Planetary Science Letters*, **302**(1):147-153.

Jerram D.A., Stollhofen H. 2002. Lava–sediment interaction in desert settings; are all peperite-like textures the result of magma–water interaction? *Journal of Volcanology and Geothermal Research*, **114**:231-249.

Katsura T., Kushiro I. 1961. Titanomaghemite in Igneous Rocks. *The American Mineralogist*, **46**:134-145.

Le Bas M.J., Le Maitre R.W., Streckeisen A., Zannetin B.A. 1986. Chemical classification of volcanic rocks based on the total alkali-silica diagram. *Journal of Petrology*, **27**(3):745-750.

Machado F.B. 2005. *Geologia e Aspectos Petrológicos das Rochas Intrusivas e Efusivas Mesozoicas de parte da borda leste da Bacia do Paraná no Estado de São Paulo*. Dissertation, Instituto de Geociências e Ciências Exatas, Universidade Estadual Paulista "Júlio de Mesquita Filho", Rio Claro, São Paulo.

Machado F.B. 2009. *Petrologia e caracterização geoquímica das fontes mantélicas da região noroeste da Província Magmática do Paraná*. PhD Thesis, Universidade Estadual Paulista "Júlio de Mesquita Filho", Rio Claro, São Paulo.

Mantovani M.S.M., Cordani U.G., Roisenberg A. 1985. Isotope geochemistry of acidic volcanics from the Parana basin and petrogenetic implications. *Revista Brasileira de Geociências*, **15**:61-65.

Marques L.S., De Min A., Rocha-Júnior E., Babinski M., Bellieni G., Figueiredo A.M.G. 2017. Elemental and Sr-Nd-Pb isotope geochemistry of the Florianopolis dyke swarm (Paraná Magmatic Province): crustal contamination and mantle source constraints. *Journal of Volcanology and Geothermal Research*. http://dx.doi.org/10.1016/j.jvolgeores.2017.07.005

Marques L.S., Dupré B., Piccirillo E.M. 1999. Mantle source compositions of the Paraná Magmatic Province: evidence from trace element and Sr-N-Pb isotope geochemistry. *Journal of Geodynamics*, **28**:439-459.

Marques L.S., Ernesto M. 2004. O magmatismo toleítico da Bacia do Paraná. *In*: Mantesso-Neto V., Bartorelli A., Carneiro C.D.R., Brito-Neves B.B. (Eds.) *Geologia do Continente Sul-Americano*: evolução da obra de Fernando Flávio Marques de Almeida. São Paulo, Beca. p. 245-263.

Marques L.S., Rocha-Júnior E.R.V., Babinski M., Carvas K.Z., Petronilho L.A., De Min A. 2016. Lead isotope constraints on the mantle sources involved in the genesis of Mesozoic high-Ti tholeiite dykes (Urubici type) from the São Francisco Craton (Southern Espinhaço, Brazil). *Brazilian Journal of Geology*, **46**:105-122.

Moraes L.C., Seer H.J. 2017. Pillow lavas and fluvio-lacustrine deposits in the northeast of Paraná Continental Magmatic Province, Brazil, *Journal of Volcanology and Geothermal Research*. http://dx.doi.org/10.1016/j.jvolgeores.2017.03.024

Morimoto N. 1988. Nomenclature of pyroxenes. *Mineralogy and Petrology*, **39**(1):55-76.

Nardy A.J.R., Enzweiler J., Bahia F.O., Oliveira M.A.F., Peneiro M.A.V. 1997. Determinação de Elementos Maiores e Menores em Rochas Silicáticas por Espectrometria de Fluorescência de Raios-X: Resultados Preliminares. *In*: VI Congresso Brasileiro de Geoquímica. *Anais...* Sociedade Brasileira de Geologia, Salvador, p. 346-348.

Pacheco F.E.R.C., Caxito F.A., Moraes L.C., Marangoni Y.R., Santos P.R.S., Pedrosa-Soares A.C. 2017. Basaltic ring structures of the Serra Geral Formation at the southern Triângulo Mineiro, Água Vermelha region, Brazil. *Journal of Volcanology and Geothermal Research*. http://dx.doi.org/10.1016/j.jvolgeores.2017.06.019

Peate D.W. 1997. The Parana-Etendeka Province. *In*: Mahoney J.J., Coffin M.F. (Eds.) *Large Igneous Provinces*: Continental, Oceanic and Planetary Flood Volcanism. Washington, D.C., American Geophysical Union. p. 217-245.

Peate D.W., Hawkesworth C.J., Mantovani M.S. 1992. Chemical stratigraphy of the Paraná lavas (South America): classification of magma types and their spatial distribution. *Bulletin of Volcanology*, **55**(1-2):119-139.

Petrelli M., Poli G., Perugini D., Peccerillo A. 2005. PetroGraph: a new software to visualize, model, and present geochemical data in igneous petrology. *Geochemistry, Geophysics, Geosystems*, **6**(7). DOI: 10.1029/2005GC000932

Piccirillo E.M., Bellieni G., Cavazzini G., Comin-Chiaramonti P., Petrini R., Melfi A.J., Pinese J.P.P., Zantedeschi P., De Min A. 1990. Lower Cretaceous tholeiitic dyke swarms from the Ponta Grossa Arch (southeast Brazil): Petrology, Sr-Nd isotopes and genetic relationships with the Paraná flood volcanics. *Chemical Geology*, **89**:19-48.

Piccirillo E.M., Melfi A.J. 1988. *The Mesozoic Flood Volcanism of the Paraná Basin: Petrogenetic and Geophysical Aspects*. São Paulo, Universidade de São Paulo.

Pinto C.P., da Silva M.A. 2014. *Mapa Geológico do Estado de Minas Gerais*, 1.1.000.000. Belo Horizonte, CODEMIG-CPRM.

Pires E.F., Guerra-Sommer M., Scherer C.M.S., Santos A.R., Cardoso E. 2011. Early Cretaceous coniferous woods from a paleoerg (Paraná Basin, Brazil). *Journal of South American Earth Sciences*, **32**:96-109.

Rao P.V.N., Swaroop P.C., Karimulla S. 2012. Mineral chemistry of Pangidi basalt flows from Andhra Pradesh. *Journal of Earth System Science*, **121**(2):525-536.

Renne P.R., Ernesto M., Pacca I.G., Coe R.S., Glen J.M., Prévot M., Perrin M. 1992. The age of Paraná flood volcanism, rifting of Gondwanaland, and the Jurassic-Cretaceous boundary. *Science*, **5084**:975-979.

Rocha-Júnior E.R.V., Marques L.S., Babinski M., Nardy A.J.R., Figueiredo A.M.G., Machado F.B. 2013. Sr-Nd-Pb isotopic constraints on the nature of the mantle sources involved in the genesis of the high-Ti tholeiites from northern Paraná Continental Flood Basalts (Brazil). *Journal of South American Earth Sciences*, **46**:9-25.

Rocha-Júnior E.R.V., Puchtel I.S., Marques L.S., Walker R.J., Machado F.B., Nardy A.J.R., Babinski M., Figueiredo A.M.G. 2012. REE Os isotope and highly siderophile element systematics of the Paraná Continental Flood Basalts (Brazil). *Earth and Planetary Science Letters*, **337/338**:164-173.

Rossetti L., Lima E.F., Waichel B.L., Hole M.J., Simões M.S., Claiton M.S., Scherer C.M.S. 2017. Lithostratigraphy and volcanology of the Serra Geral Group, Paraná-Etendeka Igneous Province in Southern Brazil: Towards a formal stratigraphic framework. *Journal of Volcanology and Geothermal Research*. http://dx.doi.org/10.1016/j.jvolgeores.2017.05.008

Sarmento C.C.T., Sommer C.A., Lima E.F. 2017. Mafic subvolcanic intrusions and their petrologic relation with the volcanism in the south hinge Torres Syncline, Parana-Etendeka Igneous Province, southern Brazil. *Journal of South American Earth Sciences*, **77**:70-91.

Scherer C.M.S. 2002. Preservation of aeolian genetic units by lava flows in the Lower Cretaceous of the Paraná Basin, southern Brazil. *Sedimentology*, **49**:97-116.

Seer H.J., Moraes L.C., Carneiro M.A. 2011. Geologia e litogeoquímica dos diques toleíticos ATi vinculados aos lineamentos magnéticos de direção NW do Arco do Alto Paranaíba em Abadia dos Dourados, MG. *In*: V Simpósio de Vulcanismo e Ambientes Associados. UFG, Goiás Velho.

Sun S.S., McDonough W.S. 1989. Chemical and isotopic systematics of oceanic basalts: implications for mantle composition and processes. *Geological Society of London Special Publications*, **42**(1):313-345.

Thiede D.S., Vasconcelos P.M. 2010. Paraná flood basalts: rapid extrusion hypothesis confirmed by new ^{40}Ar/^{39}Ar results. *Geology,* **38**(8):747-750.

Turner S., Regelous M., Kelley S., Hawkesworth C.J., Mantovani M. 1994. Magmatism and continental break-up in the South Atlantic: high precision 40Ar-39Ar geochronology. *Earth and Planetary Science Letters,* **121**:333-348.

Vernon R.H. 2004. *A Practical Guide to Rock Microstructure.* Cambridge, United Kingdom at the University Press.

Waichel B.L. 2006. *Estruturação de Derrames e Interações Lava-Sedimento na Porção Central da Província Basáltica Continental do Paraná.* PhD Thesis, Universidade Federal do Rio Grande do Sul, Porto Alegre, Rio Grande do Sul.

Wilson M. 2007. *Igneous Petrogenesis:* a global tectonic approach (10th ed.). The Netherlands, Springer.

Yavuz F. 2013. WinPyrox: a Windows program for pyroxene calculation classification and thermobarometry. *American Mineralogist,* **98**:1338-1359.